Cosmic Birefringence: Insights on Axiverse and Domain walls with CMB polarization

Silvia Gasparotto (IFAE)

Based on 2306.16355 with E. Sfakianakis
And 2311.xxxx with R.Ferreira, T.Hiramatsu, I.Obata, O.Pujolas

16/11/2023 Stockholm

Institut de Física d'Altes Energies
Generalitat de Catalunya Departament de Recerca i Universitats
Universitat Autònoma de Barcelona
Agència de Gestió d'Ajuts Universitaris i de Recerca AGAUR

Outlook of the talk

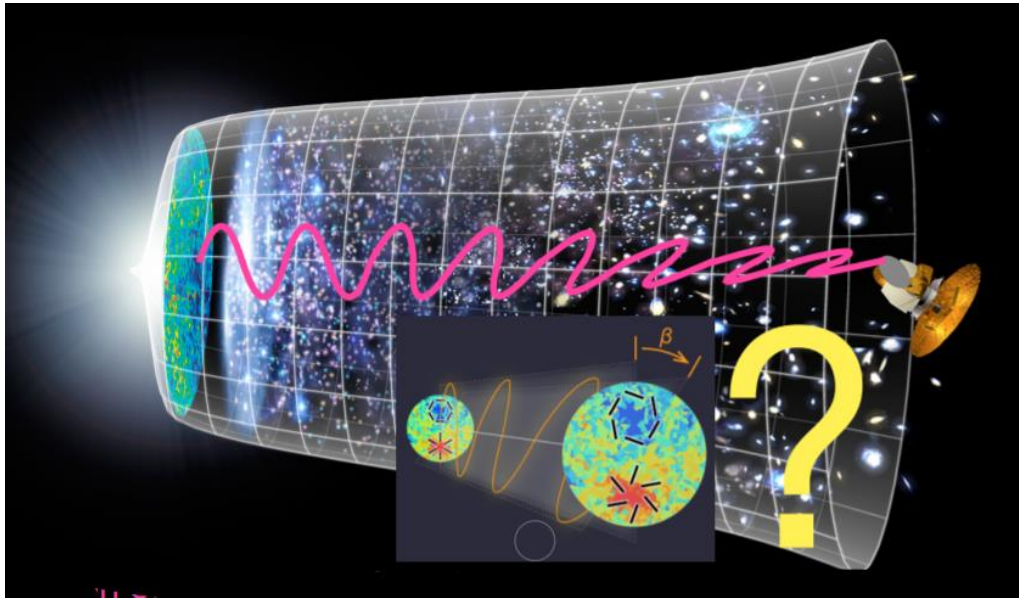

Explanation Beyond the Standard Model:
AXIONS

What's Cosmic Birefringence?

Implication for the Axiverse

Based on 2306.16355 with E. Sfakianakis

Case of Axion Domain wall

Ongoing work with R.Ferreira, T.Hiramatsu, I.Obata, O.Pujolas

The Universe filled with a «Birefringence material»

Carroll, Field & Jackiw(1990); Harari & Sikivie (1992); Carroll (1998)

If the Universe is filled with a pseudo-scalar field (e.g. axion field) coupled to the electromagnetic tensor via the Chern-Simons coupling

Turner & Widrow (1988)

the effective Lagrangian for axion electrodynamics is

Chern-Simons term

$$\mathcal{L} = -\tfrac{1}{2}\partial_\mu\theta\partial^\mu\theta - \tfrac{1}{4}F_{\mu\nu}F^{\mu\nu} + \boxed{g_a\theta F_{\mu\nu}\tilde{F}^{\mu\nu}}, \qquad (3.7)$$

$$\tilde{F}^{\mu\nu} = \sum_{\alpha\beta}\frac{\epsilon^{\mu\nu\alpha\beta}}{2\sqrt{-g}}F_{\alpha\beta}$$

where g_a is a coupling constant of the order α, and the vacuum angle $\theta = \phi_a/f_a$ (ϕ_a = axion field). The equations

$$\mathcal{L}_{\rm int} \ni \frac{1}{4}g_{\phi\gamma}\phi F_{\mu\nu}\tilde{F}^{\mu\nu} \to g_{\phi\gamma}\phi\vec{E}\cdot\vec{B}$$

<u>Parity-odd term</u>

Modification of the Maxwell equations:

$$A''_\pm(\eta,k) + \underbrace{k^2\left(1 \mp \frac{g_{\phi\gamma}\phi'}{k}\right)}_{\omega_\pm^2} A_\pm(\eta,k) = 0$$

Left and Right handed photons travel with different speed, at first order:

$\omega_\pm \simeq k \mp \frac{g_{\phi\gamma}}{2}\phi'$

- Frequency independent
- $\phi' \neq 0$

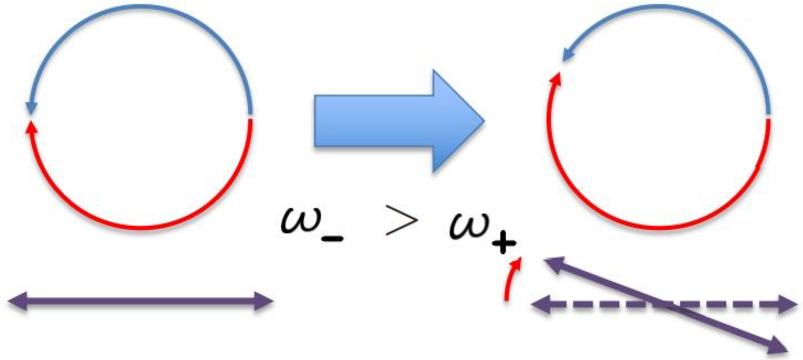

What is *Cosmic Birefringence*?

Carroll, Field & Jackiw(1990); Harari & Sikivie (1992); Carroll (1998)

The direction of linear polarization gets rotated by:

$$\beta(\hat{n}) = \frac{1}{2}\int_{\eta_{em}}^{\eta_{obs}} d\eta(\omega_- - \omega_+) = \frac{g_{\phi\gamma}}{2}\int_{\eta_{em}}^{\eta_{obs}} d\eta \frac{d\phi}{d\eta}$$

Target: CMB photons emitted 13.8 billion years ago
Lue, Wang & Kamioniski (1997); Feng et al. (2005,2006); Liu, Lee & Ng (2006)

For a uniform rotation of the polarization plane of the CMB photons, the observed polarization states E & B get modified

$$E_{l,m}^{obs} = E_{l,m}\cos(2\beta) - B_{l,m}\sin(2\beta)$$
$$B_{l,m}^{obs} = E_{l,m}\sin(2\beta) + B_{l,m}\cos(2\beta)$$

This leads to non-zero parity-odd correlations

$$C_l^{EB,obs} = \frac{1}{2}\sin(4\beta)\left(C_l^{EE} - C_l^{BB}\right) + \cancel{C_l^{EB}}\cos(4\beta)$$

=0 in standard scenario

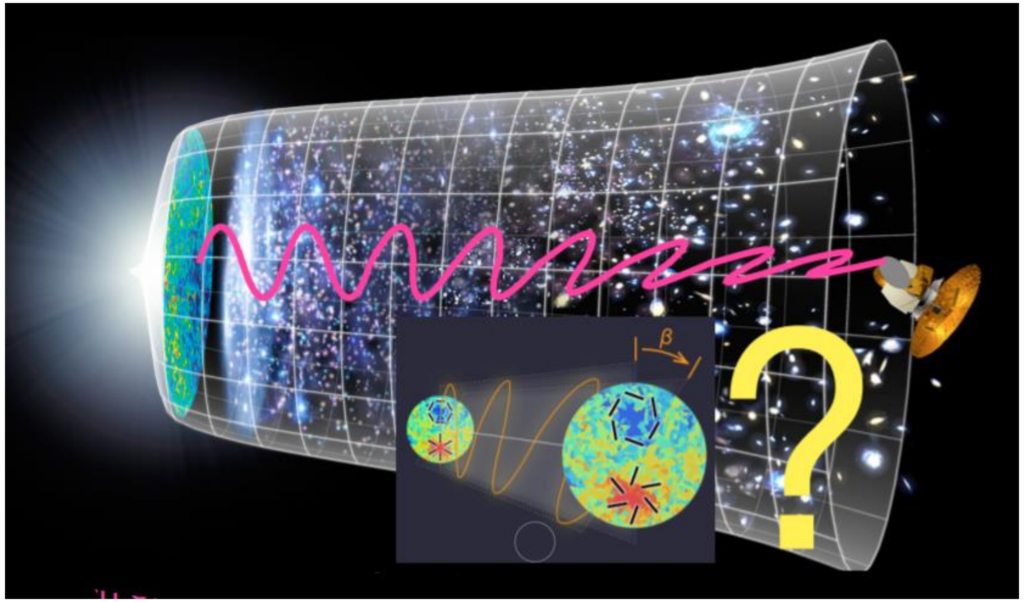

The birefringence angle β is degenerate with a miscalibration angle

Minami and Komatsu (2020) developed a new method to measure β and the miscalibration angle simultaneously → $\beta = 0.35 \pm 0.14$ deg

Hint of Parity-Violating physics: Axions

$\beta = 0.30 \pm 0.11$ deg $\quad (68\% CL)$ Diego-Palazuelos et al. (2022): applied to PR4 Planck data, modelling the polarized dust (greatest uncertainty) gives $\beta = 0.36 \pm 0.11$ deg at more than 3 σ.

$\beta = 0.33 \pm 0.10$ deg $\quad (68\% CL)$ Eskilt (2022): PR4 Planck data with low frequency map. Frequency dependence of the signal $\beta \propto \nu^n \longrightarrow n = -0.35^{+0.48}_{-0.47}$

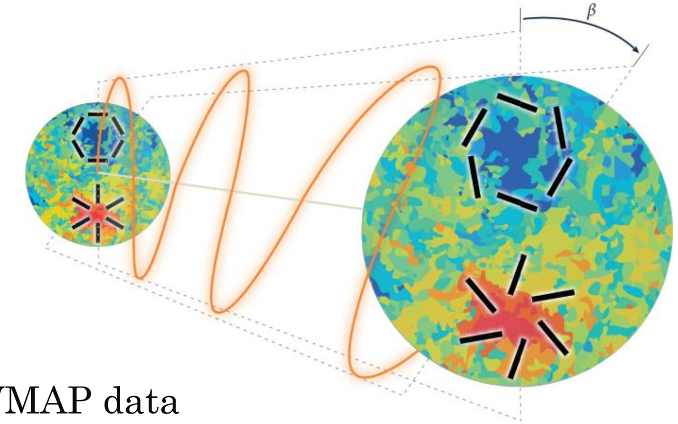

$$\boldsymbol{\beta = 0.342^{+0.094}_{-0.091} \mathbf{deg}\ (3.6\sigma)}$$

J. R. Eskilt et al (2023)
Joint analysis of Planck and WMAP data

Zero is excluded at 99.987% C.L. and compatible with *frequency independent* signal

With the increase of sensibility, the confidence of detection is also increasing!

$\Longrightarrow$ Hint of **Parity-violating** physics consistent with axion explanation!

We can test axion models of dark matter and dark energy

Birefringence and axion parameter space

$$\beta(\hat{n}) = \frac{1}{2}\int_{\eta_{em}}^{\eta_{obs}} d\eta(\omega_- - \omega_+) = \frac{g_{\phi\gamma}}{2}\int_{\eta_{em}}^{\eta_{obs}} d\eta\,\frac{d\phi}{d\eta} = \frac{g_{\phi\gamma}}{2}\left(\phi_{obs}(\hat{n}) - \phi_{em}(\hat{n})\right)$$

Axion-photon coupling

Field displacement

T. Fujita et al. (2020)

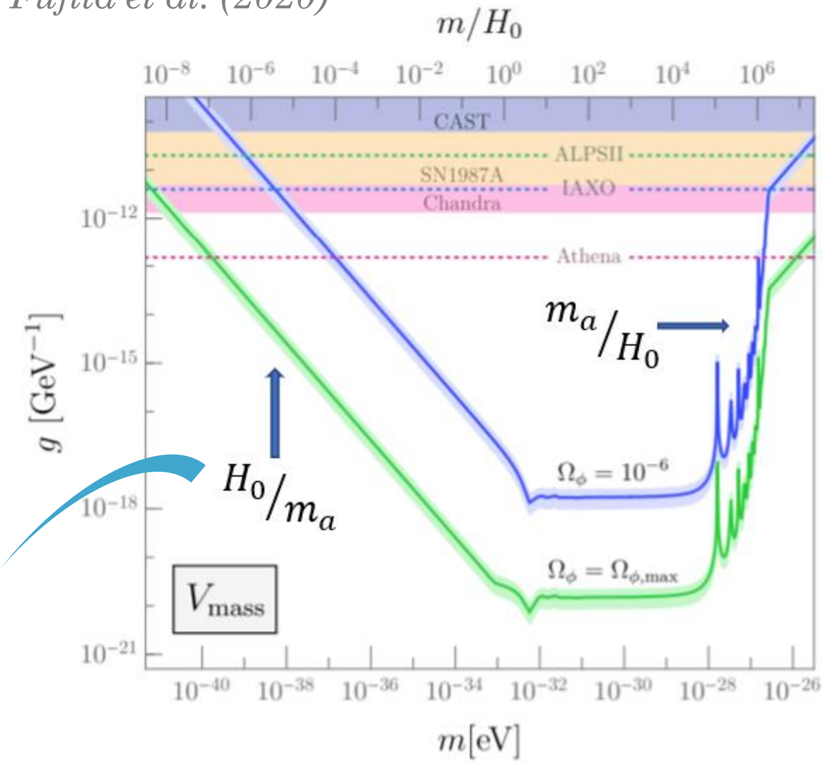

$$g_{\phi\gamma} = \frac{2\beta}{\Delta\phi}$$

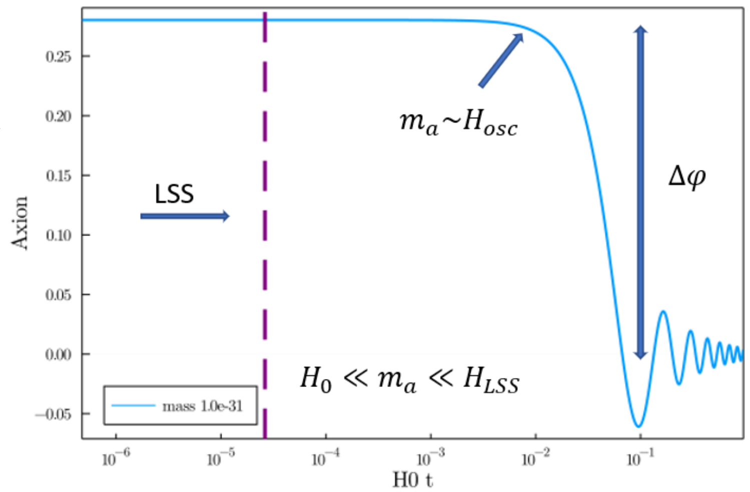

Take-home message: Axions within 15 orders of magnitude could explain the same* signal → AXIVERSE

Signal maximized for $10^{-33}\text{eV} \leq m_a \leq 10^{-29}\text{eV}$

**Sensitive to EOS of Dark Energy!*

SG & Ippei Obata 2203.09409

Part I: Cosmic Birefringence from the Axiverse

String Axiverse

Arvanitaki, Dimopoulos, Dubovsky, Kaloper, March-Russell (2009)

String Theory predicts many axions distributed over many orders of magnitude in mass and decay constant around GUT scale:

This discussion then suggests the following scenario for the distribution of f_a and m for different axions. The values of f_a are inversely proportional to the area of the corresponding cycle, so they do not change much from one axion to another. Given that the compactification is such that $S \gtrsim 200$ for string contributions to the QCD axion, and no special fine tuning is allowed, *all* axion decay constants in this scenario are likely to be close to the GUT scale $M_{GUT} \simeq 2 \times 10^{16}$ GeV. On the other hand, axion masses are exponentially sensitive to the area of the cycles, so that we expect their values to be homogeneously distributed on a log scale. Given that, as argued above, one can expect several hundred different cycles this suggests that there may be several string axions per decade of energy. It has also been argued recently that the mixing of axions

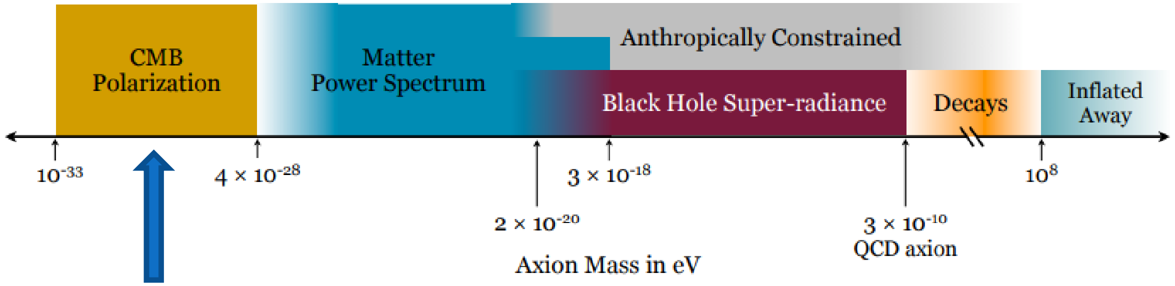

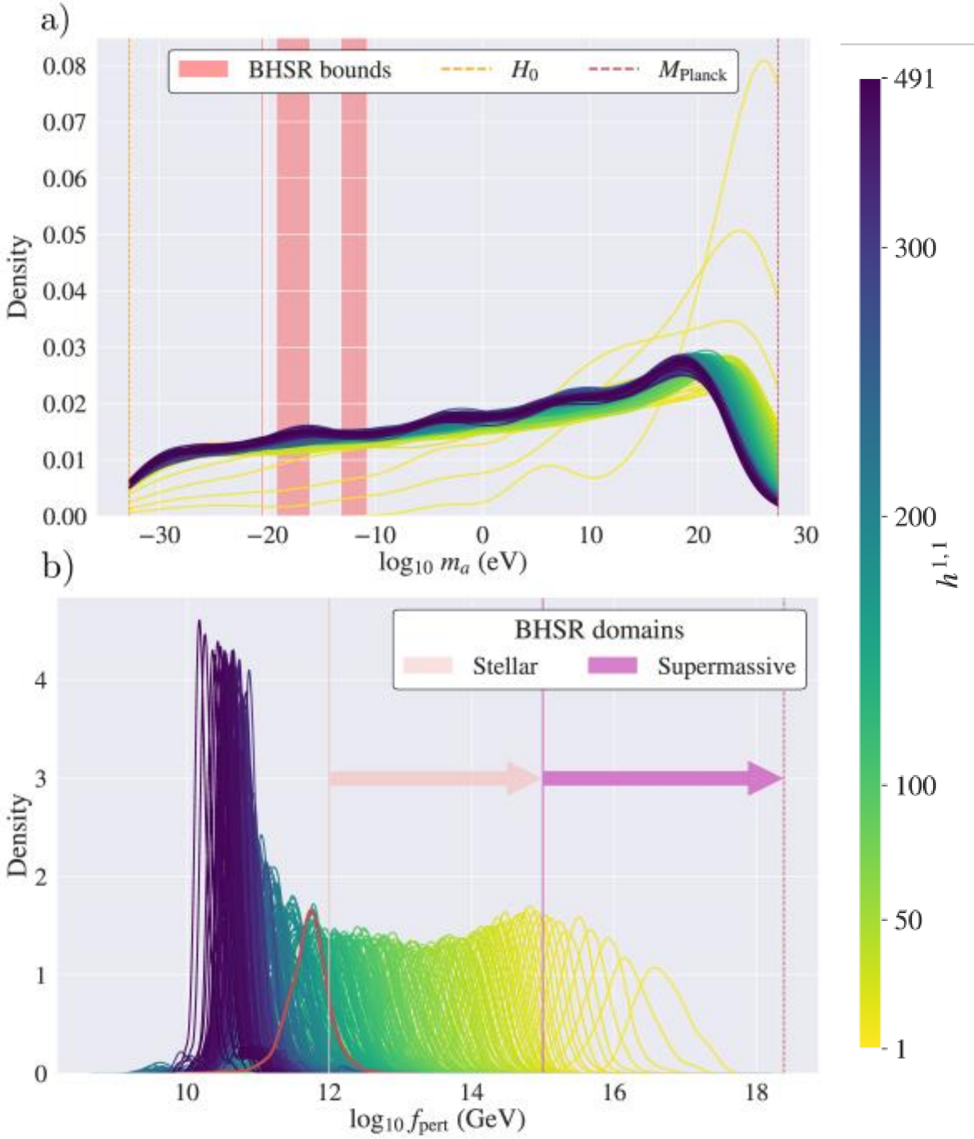

Emergent PDFs for the mass and the decay constant

Mehta et al (2021)

Toy Model: Cosine Potential

Total Birefringence angle:

$$\beta = \sum_{i=0}^{N} \frac{\alpha_{em}}{2\pi f_{a,i}} \frac{\phi_{in,i}}{2} \quad \text{with} \quad g_{\phi\gamma,i} = \frac{\alpha_{em}}{2\pi f_{a,i}}$$

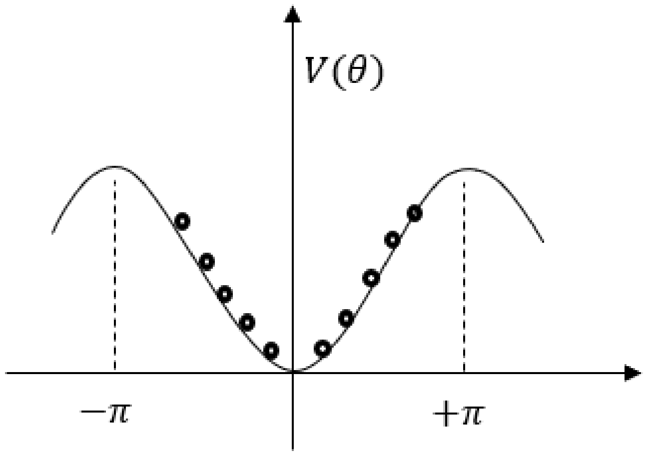

With uniform initial conditions $\theta_i = \frac{\phi_i}{f_{a,i}} \in [-\pi, \pi]$

$\langle\beta\rangle = 0$ the mean is zero,

but the VARIANCE grows with $\sqrt{N}$

$$\sqrt{\langle\beta^2\rangle} = \frac{\alpha_{em}}{4\pi} \sqrt{\sum_{i=1}^{N} \vartheta_i^2} = 0.06\sqrt{N}\ \mathrm{deg} \quad \rightarrow \beta \sim 0.3\ \mathrm{deg}$$

$$N(10^{-33}\mathrm{eV} \leq m_a \leq 10^{-29}\mathrm{eV}) = 25 \quad \rightarrow N_{dec} = 6$$

Statistical treatment of β is ok!

Note: $N_{tot} \simeq N_{dec} \times \log\frac{m_{max}}{m_{min}} = 6 \times \log\frac{M_{pl}}{H_0} = 360$

This is assuming no mixing between different axions and $c_i \sim 1$... (in "Glimmers from the Axiverse" c_i depends on the mass)

We move to the quadratic potential and then consider the Monodromy potential

Probability distributions of m_a, f_a, ϕ_{in}

- Initial field value follows a Gaussian distribution $N(0, \sigma_\phi)$ with $\sigma_\phi \sim H_{inf}$
- Gaussian distribution in log-space for the decay constant
- Probability density function (PDF) of the mass within $H_0 \leq m_a \leq M_{Pl} \rightarrow$ almost flat at very low masses
- Presence of correlations between model parameters (field that couples to $F_{\mu\nu}$ doesn't have to be an eigenvector of the mass matrix)

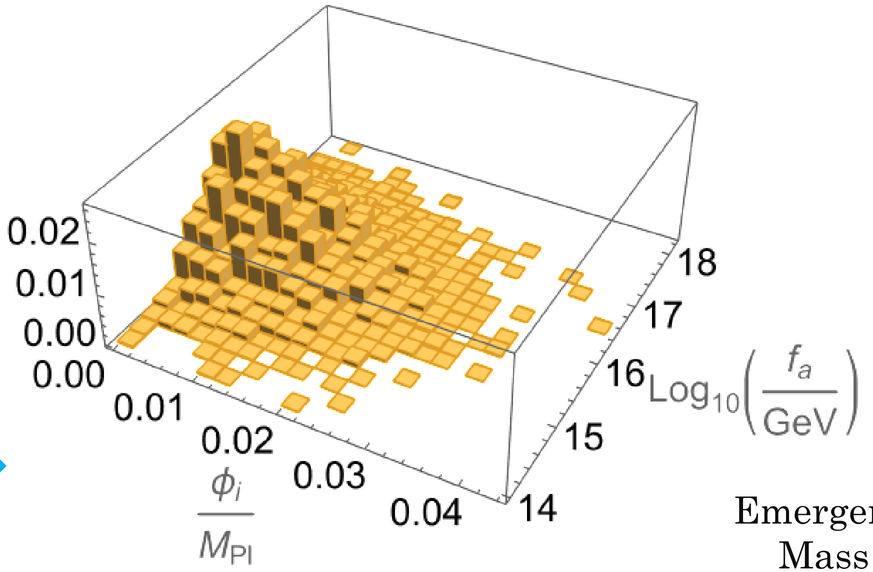

Emergent correlation between Mass and decay constant $\rho(m_a, f_a) \sim 0.5$ *Mehta et al (2021)*

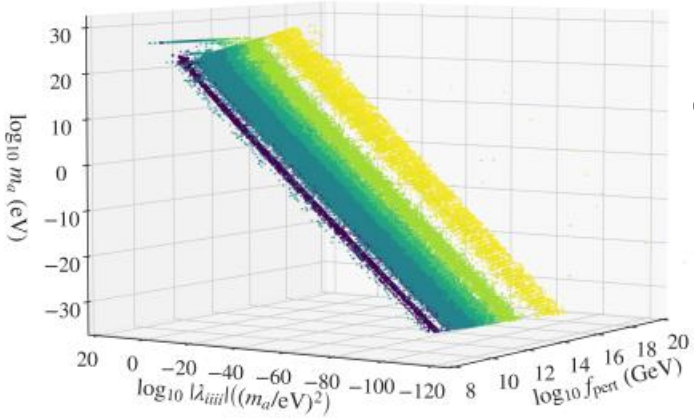

Mehta et al (2021)

Gendler, Marsh, McAllister & Moritz (2023)
Found that axion-photon coupling is more suppressed at lower masses

Correlations are important!

Implications for the Quadratic Potential

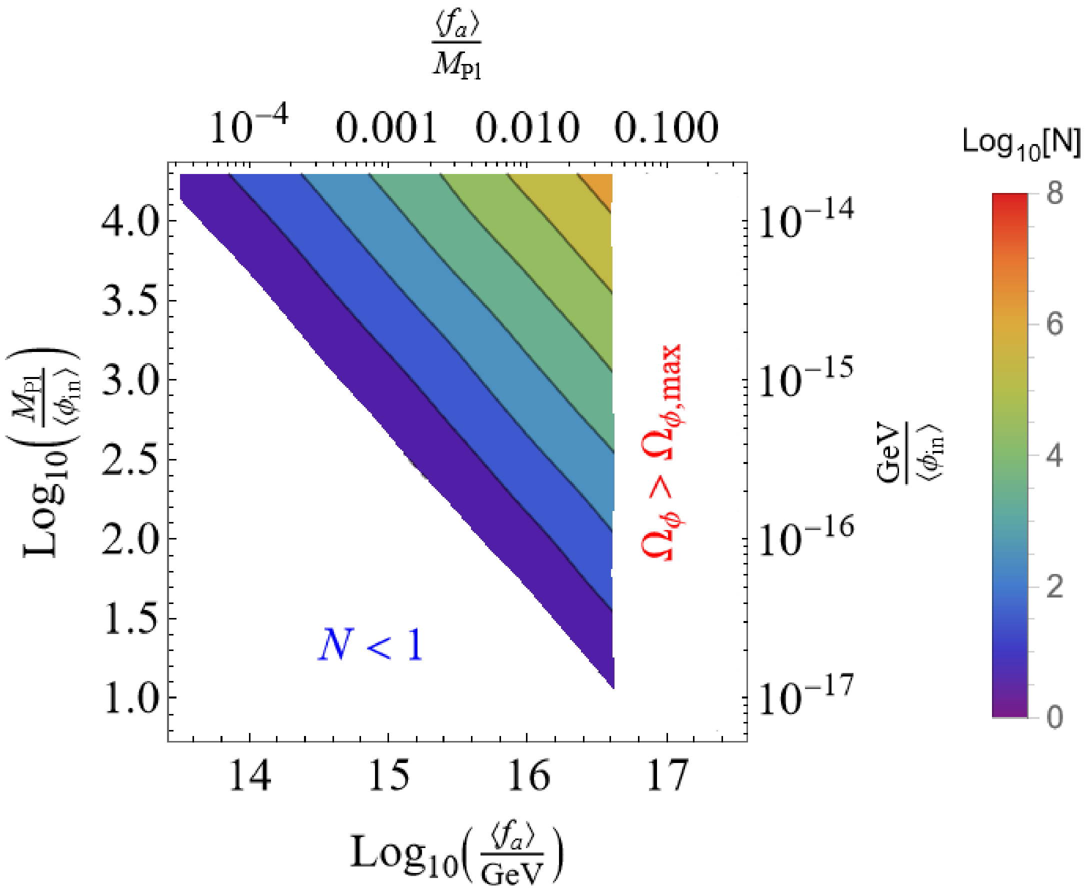

The constraint comes from the different scaling of β and Ω_ϕ

$$\beta \approx \sigma_\beta \approx 0.033\sqrt{N}\frac{\sigma_\phi}{\langle f_a\rangle}\ \mathrm{deg}$$

Enforcing $\beta\sim 0.3$ deg, $N\sim 100\left(\frac{\langle f_a\rangle}{\sigma_\phi}\right)^2$

Inserting into the axion abundance:

$$\Omega_\phi \cong \frac{3}{8}\frac{\sigma_\phi^2}{M_{pl}^2}\sum_{i=1}^{N}\frac{\phi_{in}^2}{\sigma_\phi^2} \cong \frac{3}{8}\frac{\sigma_\phi^2}{M_{pl}^2}N \sim \frac{75}{2}\left(\frac{\langle f_a\rangle}{M_{pl}}\right)^2$$

Asking $\Omega_\phi \le \Omega_{\phi,\max}$ a few percent of DM gives an

upper bound on the decay constant!

Implications for the Quadratic Potential

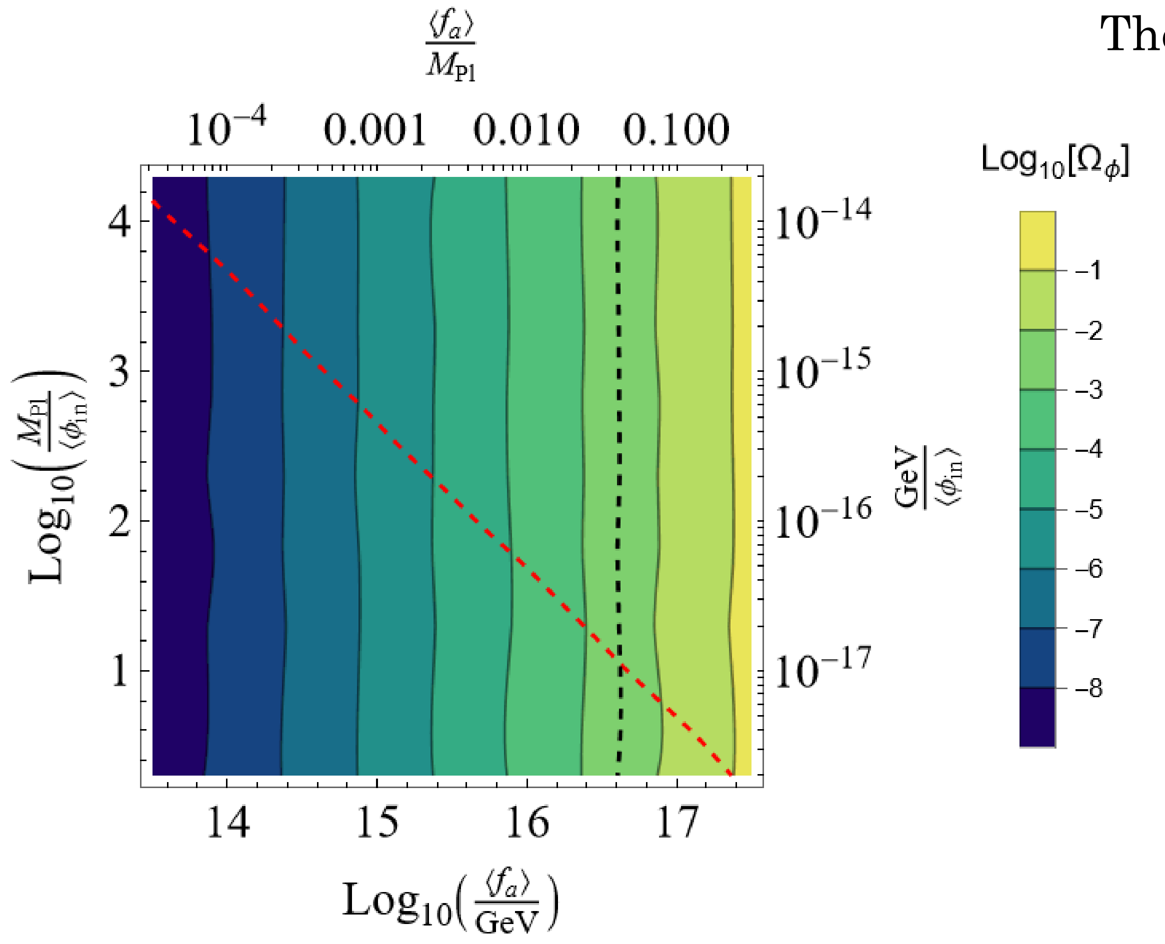

The constraint comes from the different scaling of β and Ω_ϕ

$$\beta \approx \sigma_\beta \approx 0.033\sqrt{N}\frac{\sigma_\phi}{\langle f_a \rangle}\ \mathrm{deg}$$

Enforcing $\beta \sim 0.3$ deg, $N \sim 100\left(\frac{\langle f_a \rangle}{\sigma_\phi}\right)^2$

Inserting into the axion abundance:

$$\Omega_\phi \cong \frac{3}{8}\frac{\sigma_\phi^2}{M_{pl}^2}\sum_{i=1}^{N}\frac{\phi_{in}^2}{\sigma_\phi^2} \cong \frac{3}{8}\frac{\sigma_\phi^2}{M_{pl}^2}N \sim \frac{75}{2}\left(\frac{\langle f_a \rangle}{M_{pl}}\right)^2$$

Asking $\Omega_\phi \leq \Omega_{\phi,max}$ a few percent of DM gives an *upper bound on the decay constant!*

Projecting the abundance at higher masses

With just the Birefringence we cannot test the mass distribution at masses $m_a \geq 10^{-28}\text{eV} \sim H_{eq}$, but assuming the same distribution on f_a and ϕ_{in} at higher masses

$$\langle \Omega_{\phi,tot} \rangle = \frac{N}{6}(9\Omega_r)^{\frac{3}{4}} \left\langle \sqrt{\frac{m}{H_o}} \right\rangle \left\langle \left(\frac{\phi_{in}}{M_{Pl}}\right)^2 \right\rangle$$

$$\rightarrow \frac{N_{dec}}{3log(10)}(9\Omega_r)^{\frac{3}{4}} \sqrt{\frac{m_{max}}{H_0}} \frac{\sigma_{phi}^2}{M_{Pl}^2} \quad with \;\; N_{dec} \sim 25 \left(\frac{\langle f_a \rangle}{\sigma_\phi}\right)^2$$

$$\langle \Omega_{\phi,tot} \rangle \rightarrow \frac{25(9\Omega_r)^{\frac{3}{4}}}{3log(10)} \sqrt{\frac{m_{max}}{H_0}} \frac{\langle f_a \rangle^2}{M_{Pl}^2}$$

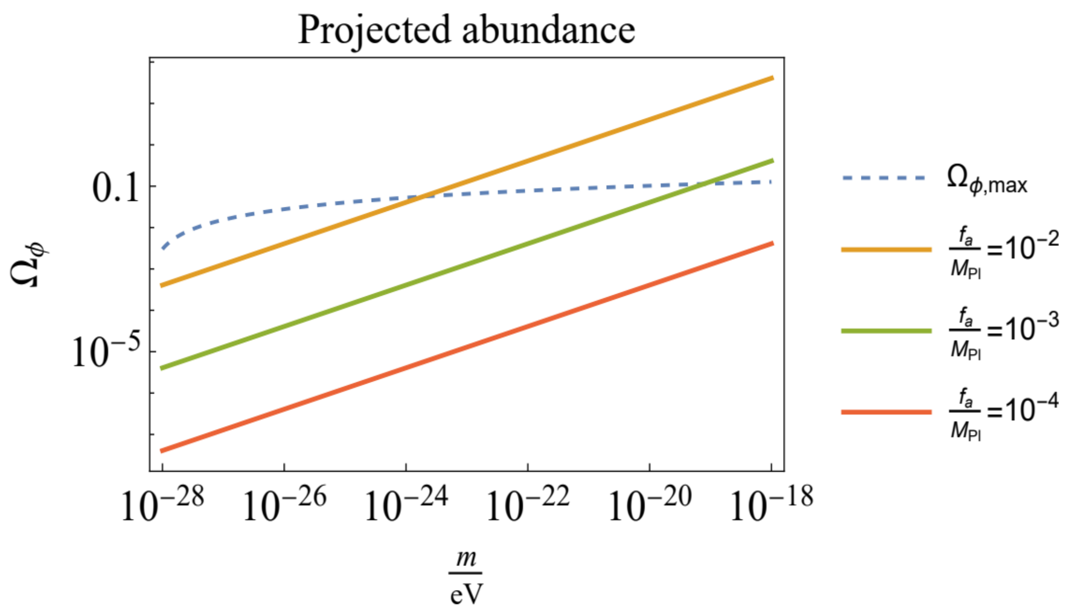

Comparing it with the current bounds on Ω_{phi} we find m_{max} that depends on $\langle f_a \rangle$!

Testing the Mass Distribution with Birefringence Tomography

Look also at B. D. Sherwin and T. Namikawa(2021), M. Galaverni et al. (2023)

The β-angle is only approximately constant, l-dependence comes from the contribution at different epochs:

1. Recombination $z \sim 1090 \rightarrow m_a \leq 3 \times 10^{-29}$ eV
2. Reionization $z \sim 7 \rightarrow m_a \leq 10^{-31}$ eV

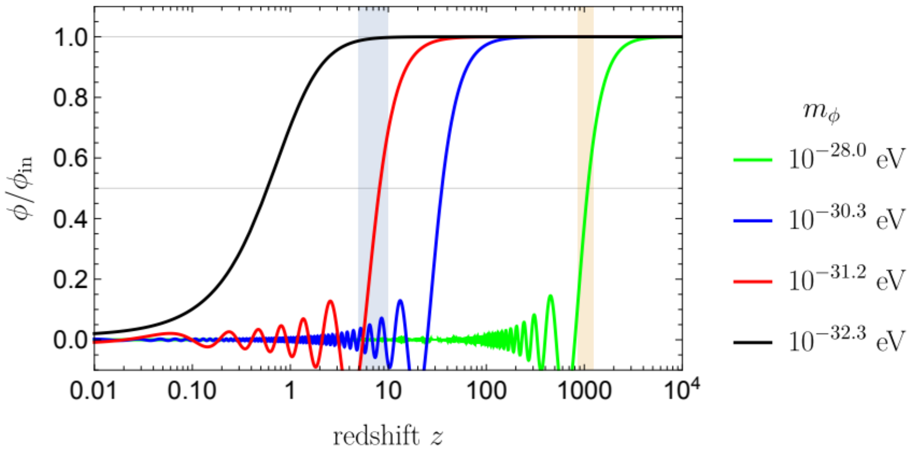

Reionization bump can probe $10^{-33} \leq m_a \leq 10^{-31}$ eV:

Hiromasa Nakatsuka et al. (2022)

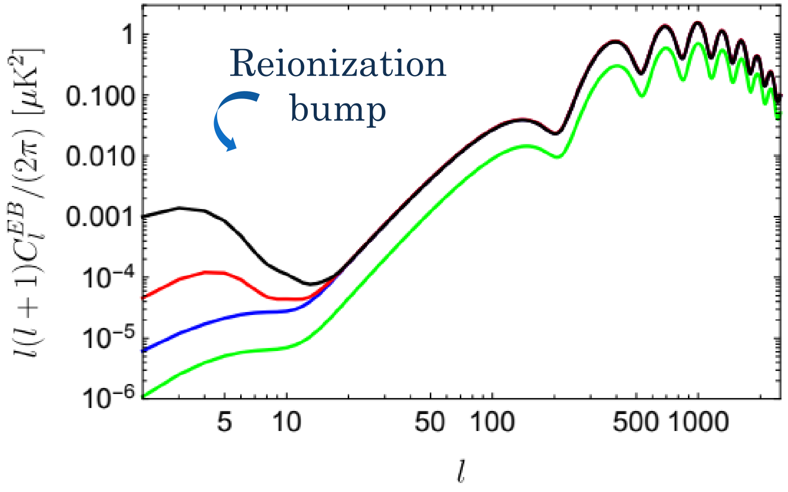

$$\frac{\beta_{rei}}{\beta_{rec}} \cong \frac{\sqrt{N_{tot}P(10^{-33} \leq m_a \leq 10^{-31}\ \mathrm{eV})}}{\sqrt{N_{tot}P(10^{-33} \leq m_a \leq 10^{-29}\ \mathrm{eV})}} \cong \frac{\sqrt{2}}{\sqrt{4}} \approx 0.7$$

Uniform mass distribution

Independent on the total number of axions across all masses!

Effect of correlations

The presence of correlations weights differently the contribution from different axions:

- $\rho(m_a, f_a) > 0 \rightarrow$ contribution from heavier axions is suppressed $\beta_{rec} \sim \beta_{rei}$
- $\rho(m_a, f_a) < 0 \rightarrow$ contribution from lighter axions is suppressed $\beta_{rec} \gg \beta_{rei}$

This changes the emergent distribution of β_{rei}/β_{rec}

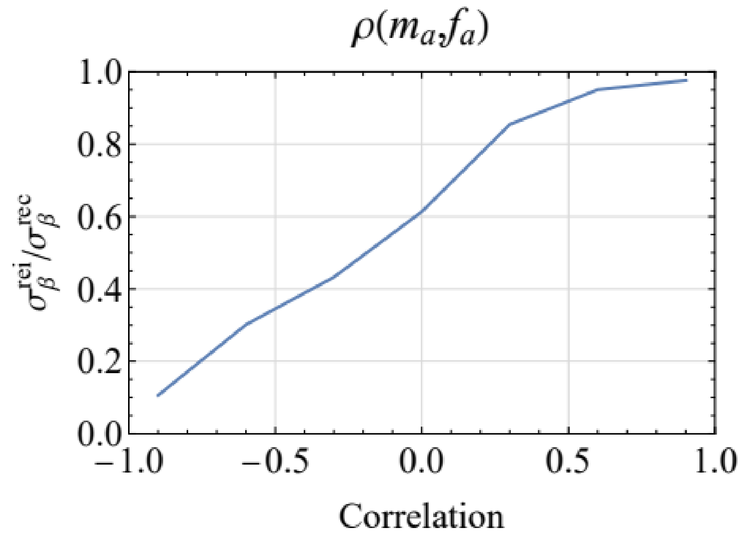

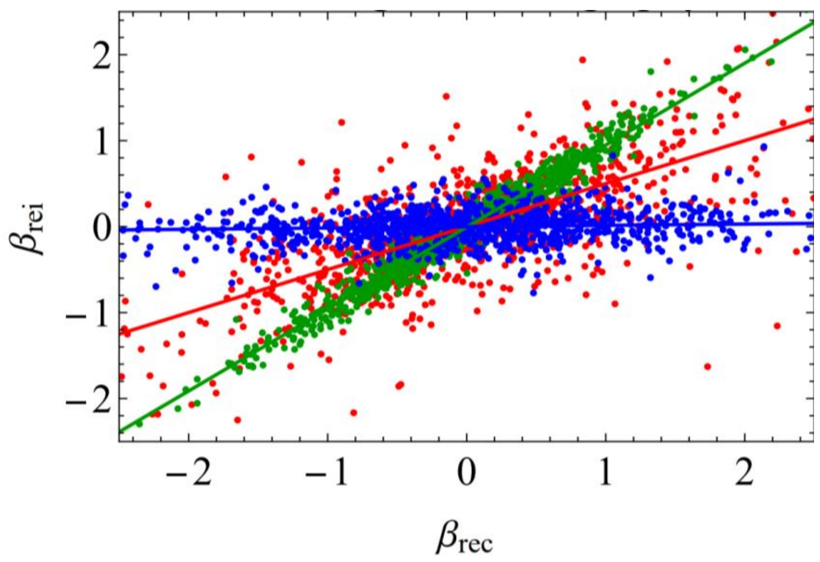

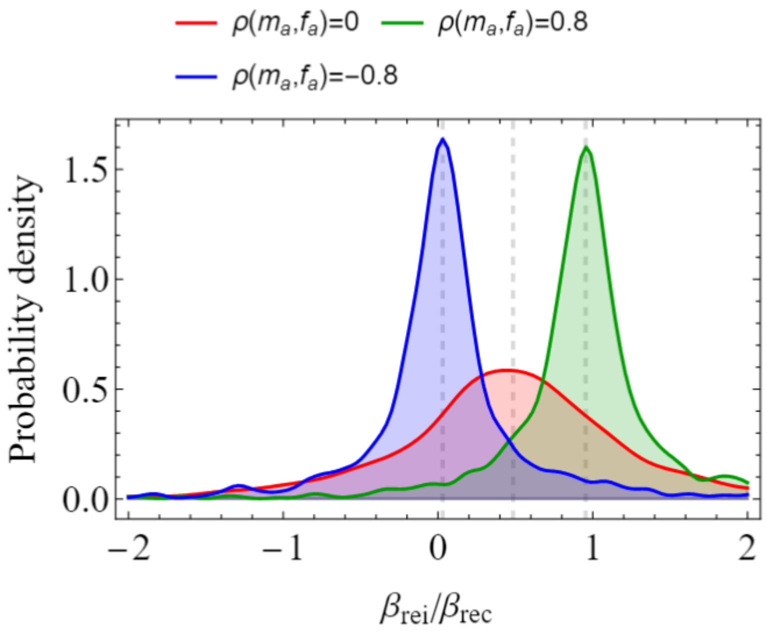

Monodromy potential

Monodromy potential, asymptotically flat at large field values

$$V(\phi) = \frac{M^2 m^2}{2p}\left[\left(1+\frac{\phi^2}{M^2}\right)^p - 1\right] \qquad p = \frac{1}{2}$$

The results change depending on the

initial condition ϕ_i, the mass m and the transition scale M

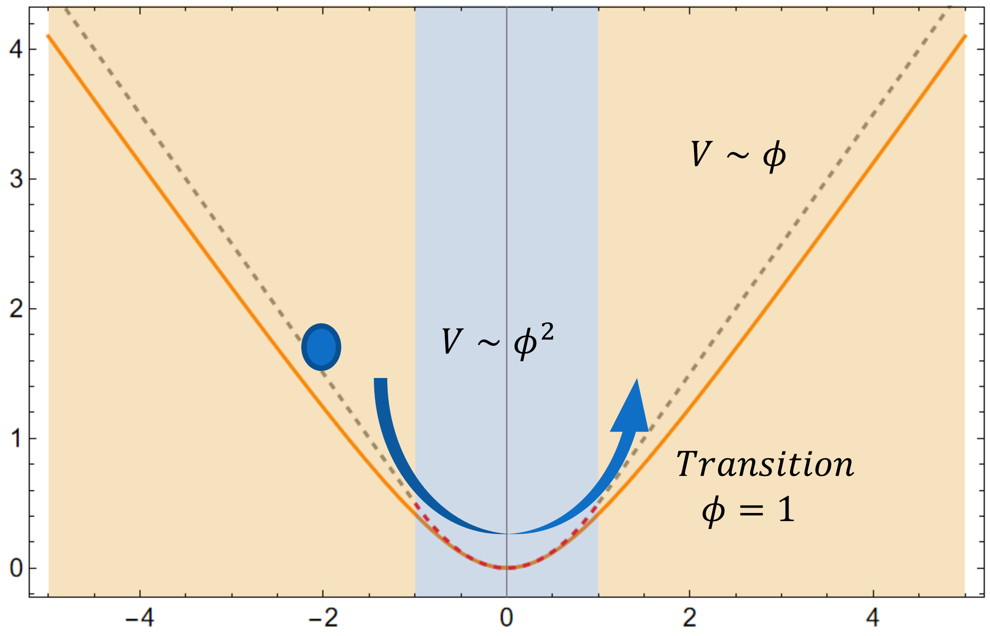

Background evolution depends on:

- Onset of oscillations $t_{osc} \sim \sqrt{\left|\frac{\phi}{V_{,\phi}}\right|}$
- Transition from linear to quadratic potential $t_1 \sim \sqrt{6(\phi_{in} - 1)}/m$

Both depends on the initial conditions!

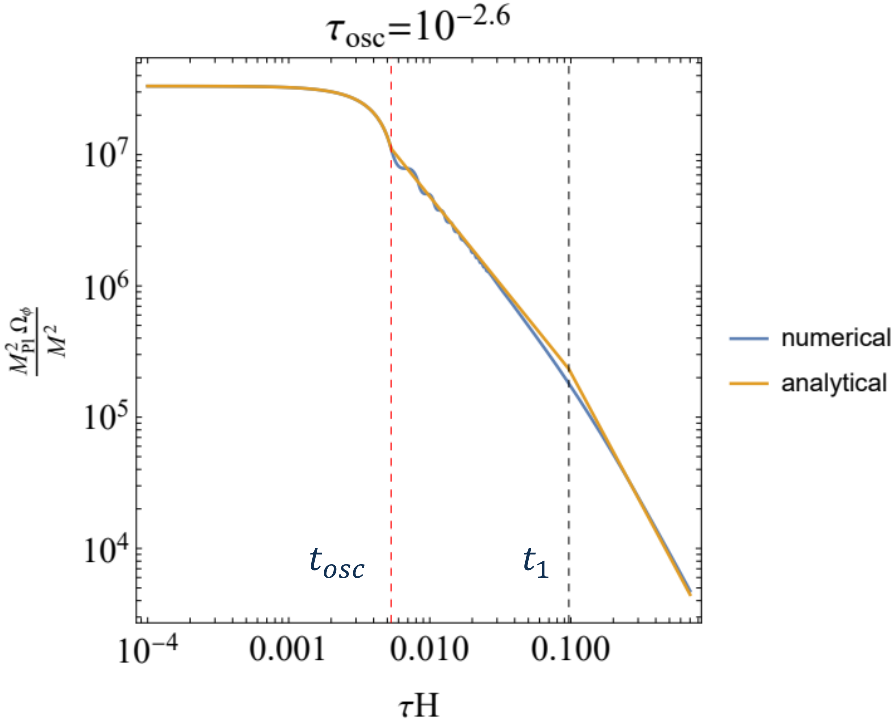

Monodromy potential

Three types of evolution: linear potential, quadratic potential and transition of behavior depending on the initial condition ϕ_{in}, the mass m and the transition scale M

In each region, the final abundance is different with respect the model parameters

$\rightarrow$ different bound on the (f_a, ϕ_{in}) plane

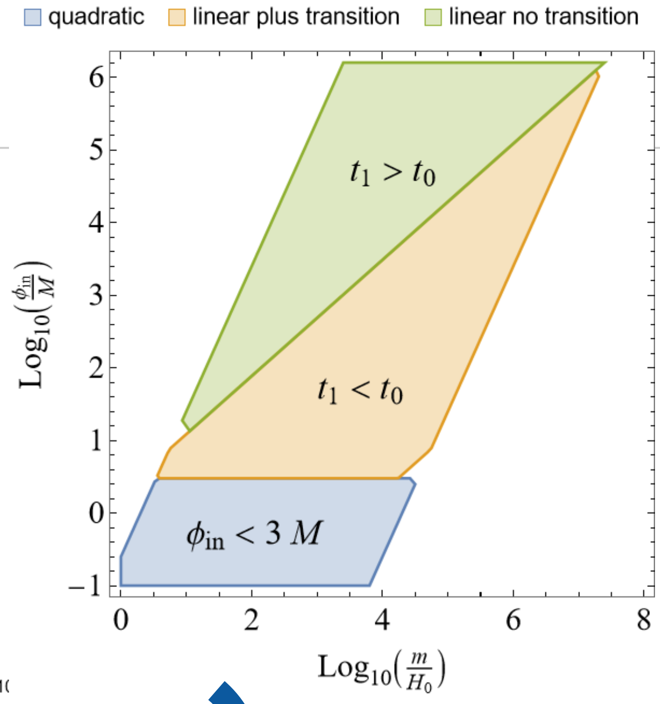

Fixing the transition scale $M = 10^{12}$ GeV

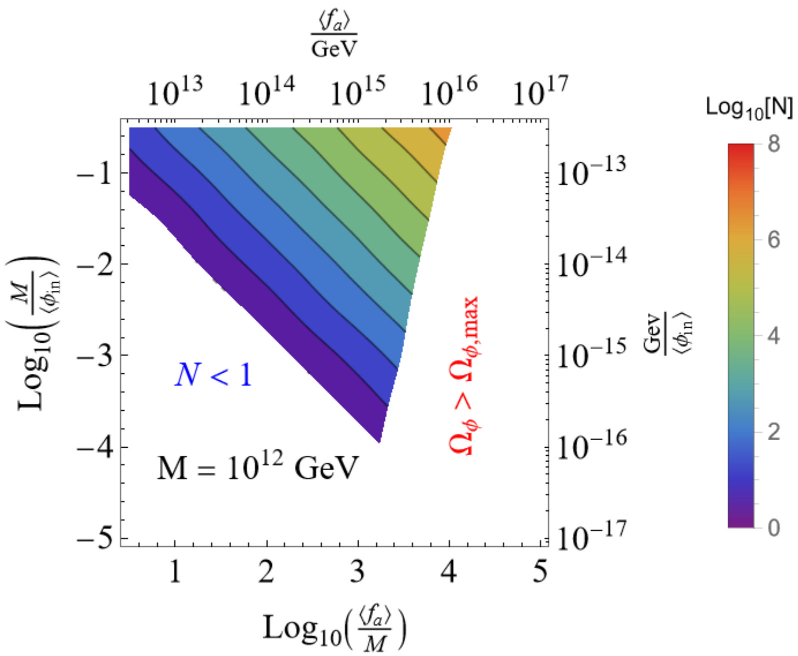

Linear plus transition

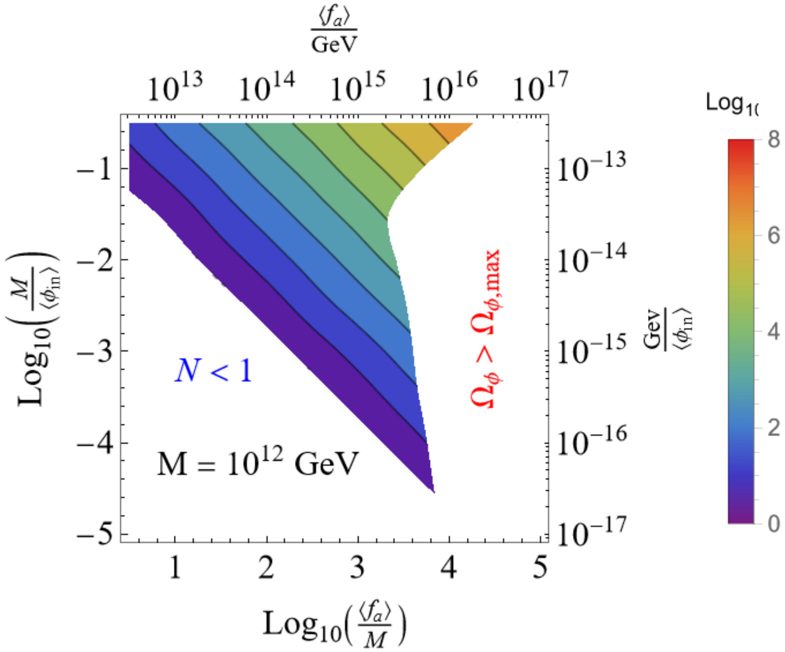

Linear no transition

Recap of Part I

- The signal can be explained with several axions per decade → depending on ϕ_{in} and f_a
- The cosmic birefringence signal and the bounds on the axion abundance constrain on the (f_a, ϕ_{in}) parameter space which depend on the axion potential ($f_a \leq 10^{17}$ GeV for quadratic)
- Expectation at higher masses of the abundance suggests a link between m_{max} and $\langle f_a \rangle$

  $m_{max} \sim 10^{-24}$eV for $\langle f_a \rangle \sim 10^{16}$GeV
- Birefringence tomography will allow testing Axiverse PDFs

  →mass distribution and presence of correlations $\rho(m_a, f_a, \phi_{in})$

Cosmic birefringence as a complementary test for the Axiverse at lower masses (lower than those accessible to Superradiance)

Part II: CB from Domain Walls

Anisotropies and Gravitational waves

Domain Walls

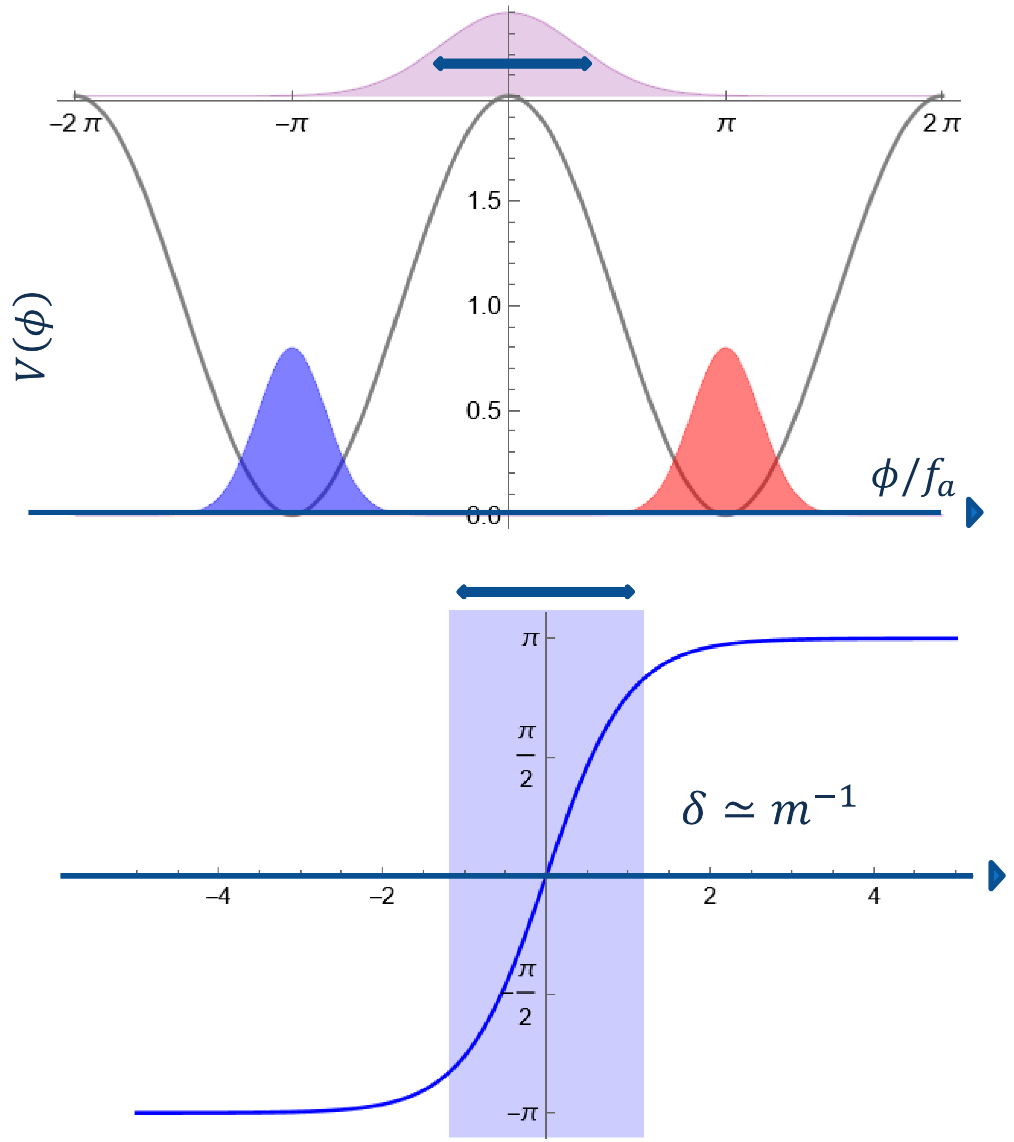

DWs: field configuration between two degenerate minima. The vacuum manifold is disconnected → natural for axions

$$V(\phi) = \frac{1}{2} m^2 f_a^2 \left[1 + \cos\left(\frac{N_{dw}\phi}{f_a}\right)\right]$$

- $H > m$ field is frozen at its initial condition (for DWs $\sigma_{\phi_{in}} \sim f_a$)
- $H \sim m$ field starts oscillating around the closest minima

DWs form when the width $\delta \simeq m^{-1}$ fits inside the Hubble horizon.

Cosmological Evolution

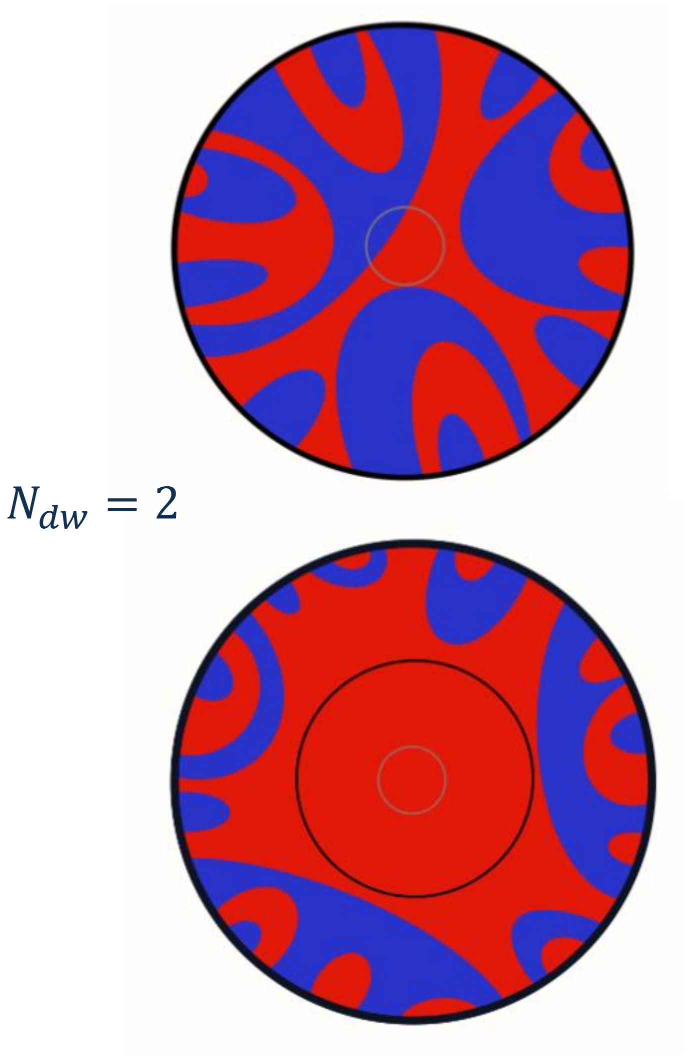

Domain walls soon reach an attractor regime, called "***scaling***"

(Press, Ryden and Spergel, 1989)

$\rightarrow O(1)$ DW for Hubble volume, $L_{dw} \sim H^{-1} \sim t$

Energy density in terms of the tension $\sigma_{dm} = m f_a^2$:

$$\rho_{dw} \sim \frac{\sigma_{dw} t^2}{t^3} \sim \frac{\sigma_{dw}}{t}$$

$\rightarrow$ decays slower than the background $(\rho_m \sim t^{-2})$

Their relative importance grows over time $\rightarrow$ Domain wall problem:

(Zel'dovich, Kobzarev and Okun, 1975)

- Collapse (potential bias)
- $\sigma < MeV^3$ (for axion $f_a < \left(\frac{10^{-27} eV}{m}\right) \times 10^{13}$ GeV)

Isotropic Cosmic Birefringence

Based on F. Takahashi and W. Yin (2021), Kitajima et al (2022),Gonzales et al (2022)

$N_{dw} = 2$

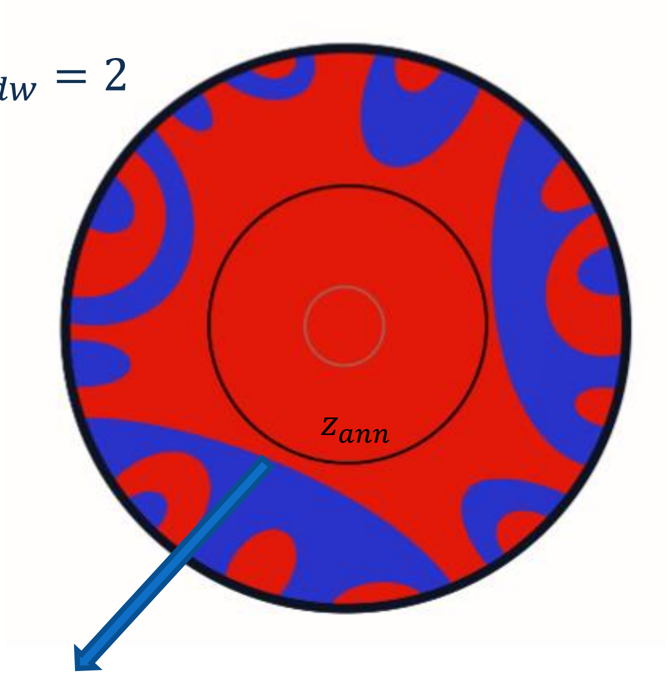

Network collapse at z_{ann}

Birefringence tomography:

- $z_{rec} > z_{ann} > z_{rei} \quad \rightarrow \beta_{rec} \neq \beta_{rei} = 0$
- $z_{ann} < z_{rei} \quad \rightarrow \beta_{rec} = \beta_{rei} \neq 0$

To contribute to CB, domain walls must be around at some point during/after recombination. Isotropic rotation is given by the average over all sky:

$$\langle \beta \rangle = \frac{\alpha_{em} c}{4\pi} (\theta_0 - \langle \theta_{LS}(\hat{n}) \rangle) = 0.21\, c \frac{\langle \Delta\theta(\hat{n}) \rangle}{2\pi}\ deg$$

With $g_{\phi\gamma} = \frac{\alpha_{em} c}{2\pi f_a}$ and $\phi = f_a \theta$, taking $\theta_0 = +\pi$

$$\langle \Delta\theta \rangle = P_+ \big(+\pi - (\pi) \big) + P_- \big(+\pi - (-\pi) \big) = \frac{1}{2} 2\pi$$

For a potential with N_{dw} minima

$$\langle \beta \rangle = 0.21\, c \left(\frac{1}{2} + \frac{1 - 2\theta_0}{N_{dw}} \right)$$

This monopole contribution comes from the symmetry breaking of the our “local” value which selects one of the many minima

Anisotropic Cosmic Birefringence

Based on F. Takahashi and W. Yin (2021), Kitajima et al (2022),Gonzales et al (2022)

Axion DWs field fluctuations are $O(1)$ per definition

- Larger anisotropies on the birefringence angle (compared to the "pre-inflationary" case where $\frac{H_I}{f_a} \ll 1$)
- Anisotropic birefringence is characterized by the power spectrum

$$C_\ell^{\beta\beta}(\eta) = \frac{4}{\pi}\beta_{iso}^2 \int \frac{dk}{k} J_\ell^2(k\Delta\eta) P_\theta(k) \quad \text{where } \beta_{iso} \simeq \frac{\alpha_{em} c}{4} \rightarrow \text{smoking gun for DW scenario!}$$

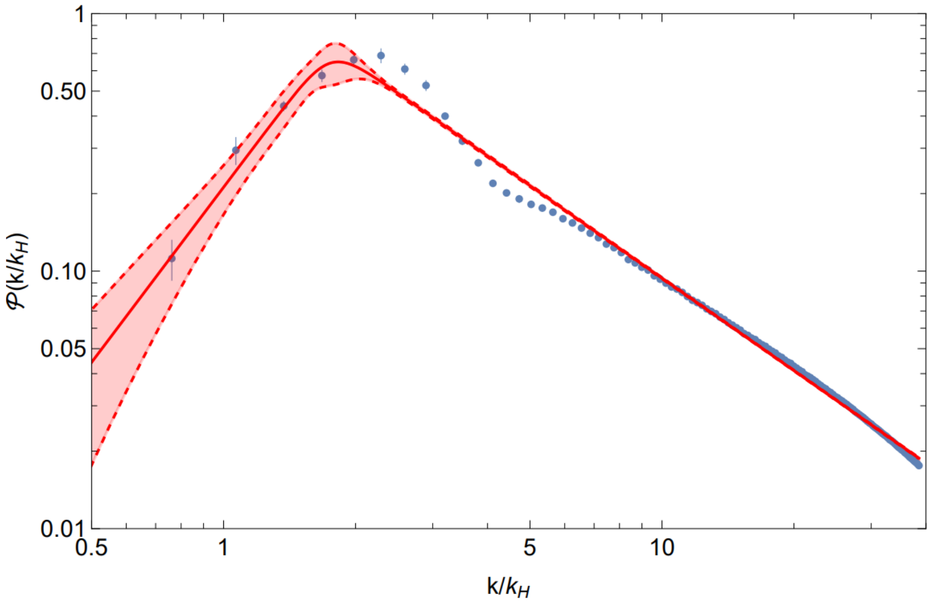

$P_\theta(k) = \frac{k^3}{2\pi}\langle\theta_k\theta_k\rangle$, scalar power spectrum:

- Domain Walls: $P_\theta(k)$ peaks at horizon size $k \sim k_H$ (doesn't depend on the initial condition)
- Before Domain Walls: spectrum highly depends on the initial conditions

DWs at recombination and reionization

Anisotropies in the scalar power spectrum translate into anisotropies in the cosmic birefringence,

$$C_\ell^{\beta\beta}(\eta) = \frac{4}{\pi}\beta_{iso}^2 \int \frac{dk}{k} J_\ell^2(k\Delta\eta) P_\theta(k)$$

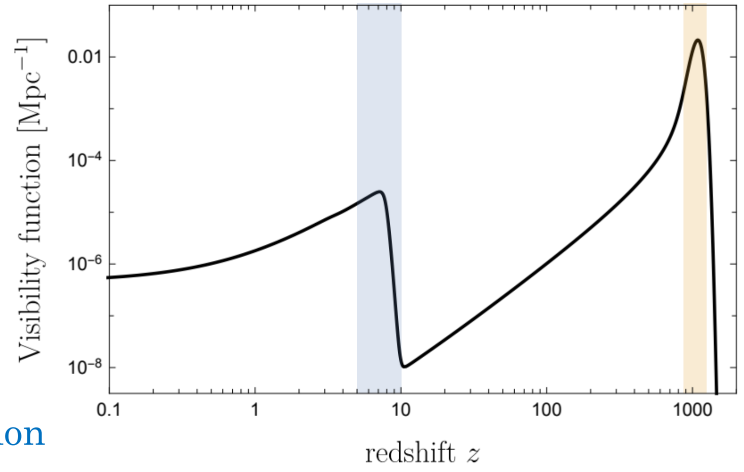

Anisotropies from recombination

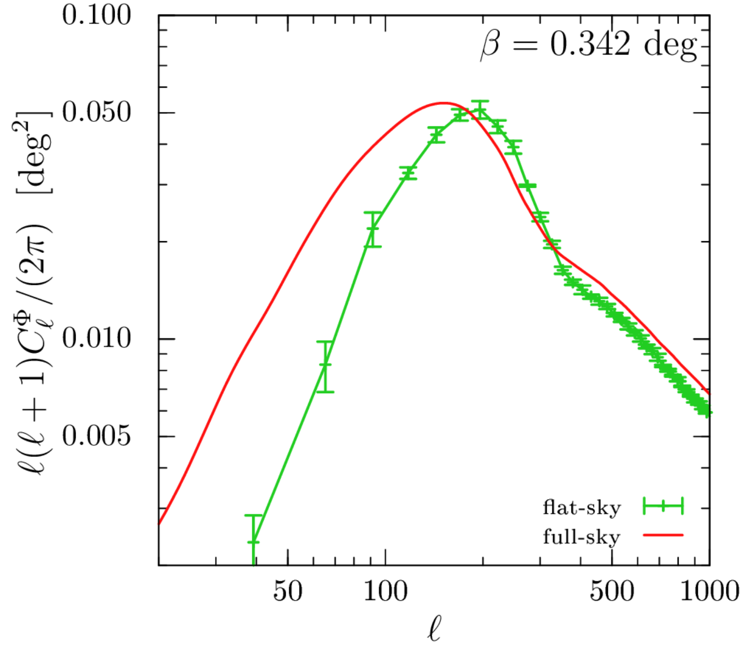

Anisotropies from reionization

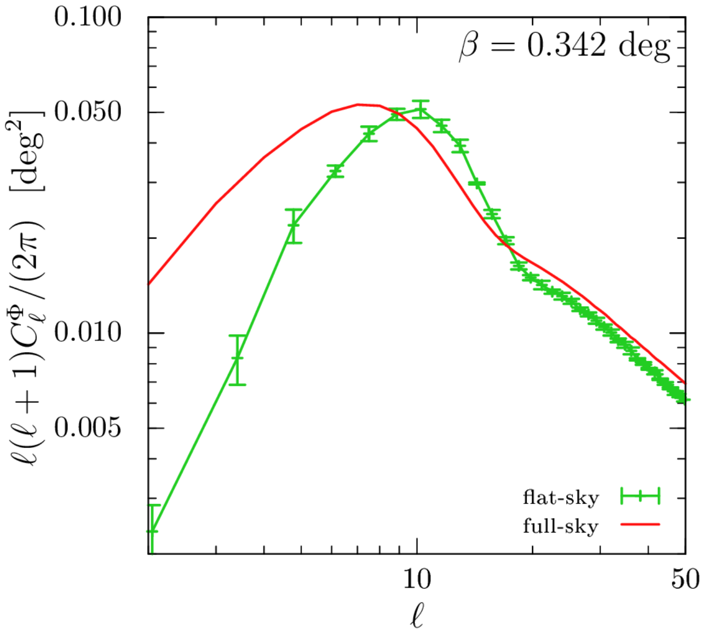

Contributions coming from the DW network at recombination and reionization which peak at different scales
→ birefringence tomography can be used to distinguish different formation/annihilation scenarios

Observable 2: Gravitational waves

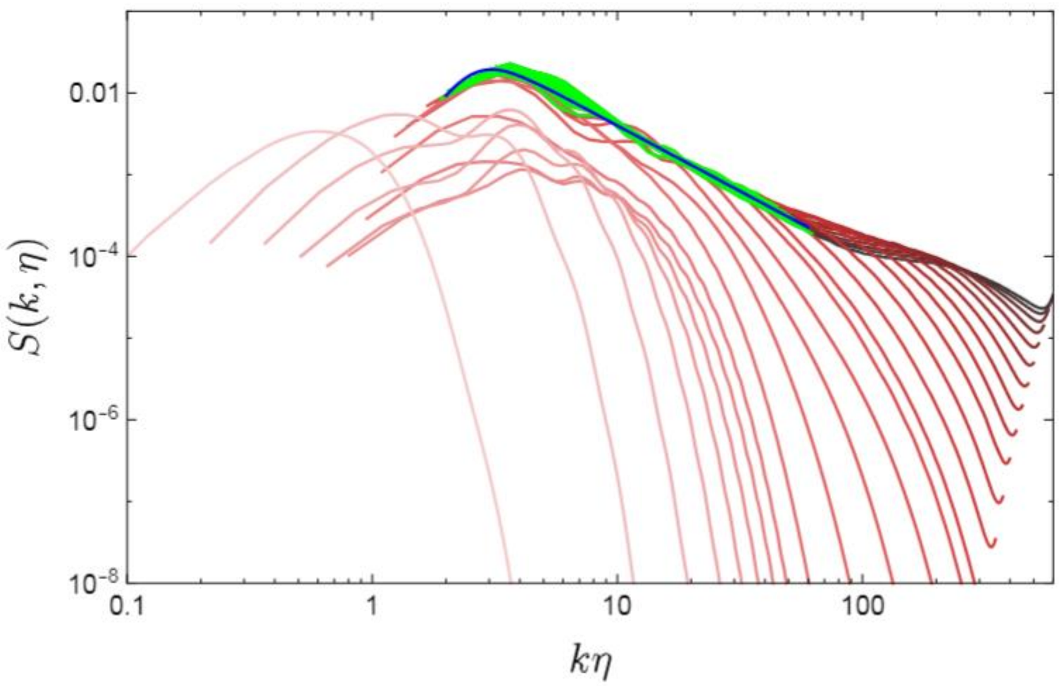

In scaling $S(k,\eta) \to S_{scal}(k\eta)$, spectrum peaks at horizon size, numerically $k\eta \sim 3$

The motion of the network generates a stochastic gravitational wave background. The basic mechanism is easy to estimate in scaling:

- Typical curvature radius $R_{dw} \sim t$ and mass $M_{dw} \sim \sigma_{dw} t^2$ of the DW
- Quadrupole $Q \sim M_{dw} R_{dw}^2 \sim \sigma_{dw} t^4 \Rightarrow$ Power in GW $P \sim G\dddot{Q}\dddot{Q} \sim \sigma_{dw}^2 t^2$

Vilenkin (1981); Preskill, Trivedi, Wilczek and Wise (1991); Gleiser and Roberts (1998)

The energy density released in GWs is

$$\rho_{GW} \sim \frac{Pt}{Vol} \sim \frac{G\sigma^2 t^3}{t^3} \sim const \quad \text{(at horizon size)}$$

$$\Omega_{GW}(\eta\, k) = \frac{1}{\rho_{tot}(\eta)} \frac{d\rho_{GW}(\eta,k)}{d\log(k)} = \left(\frac{\rho_{dw}}{\rho_{tot}}\right)^2 S(k,\eta)$$

B-modes of CMB

The relative abundance of the DW increases over time:

→ the dominant contribution of the GW spectrum comes from later times

→ for annihilating network $z_{ann} \leq z_{rec}$, the spectrum peaks at $k_{peak} \sim \frac{3}{\eta_{peak}}$

Current and future CMB constraint on the stochastic GW background from Namikawa et all, 1904.02115

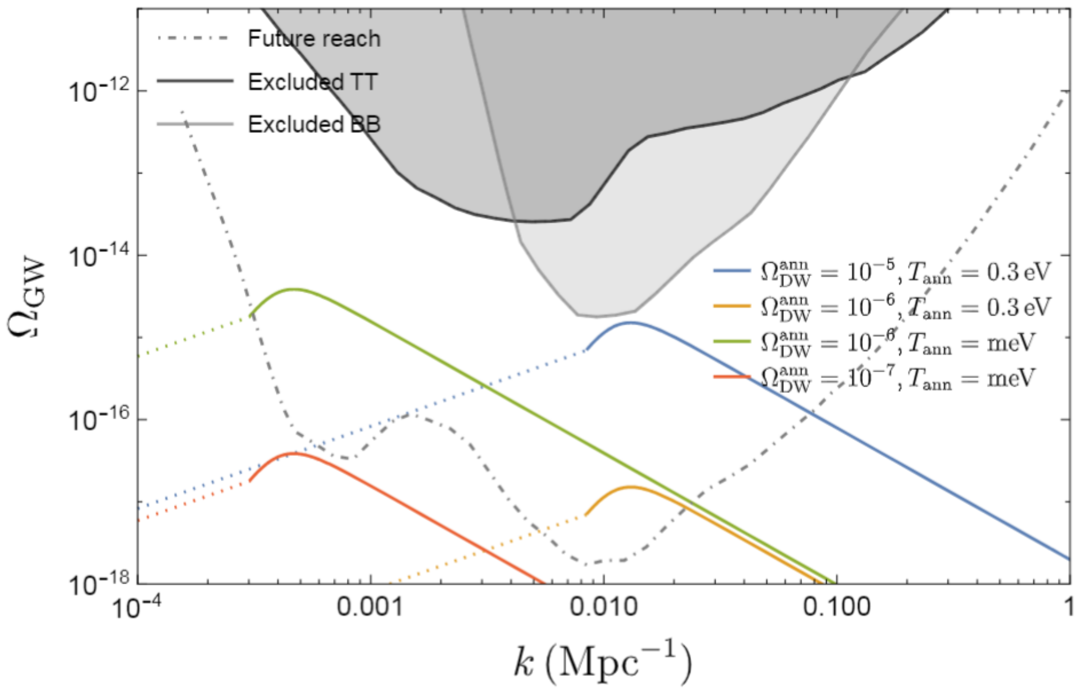

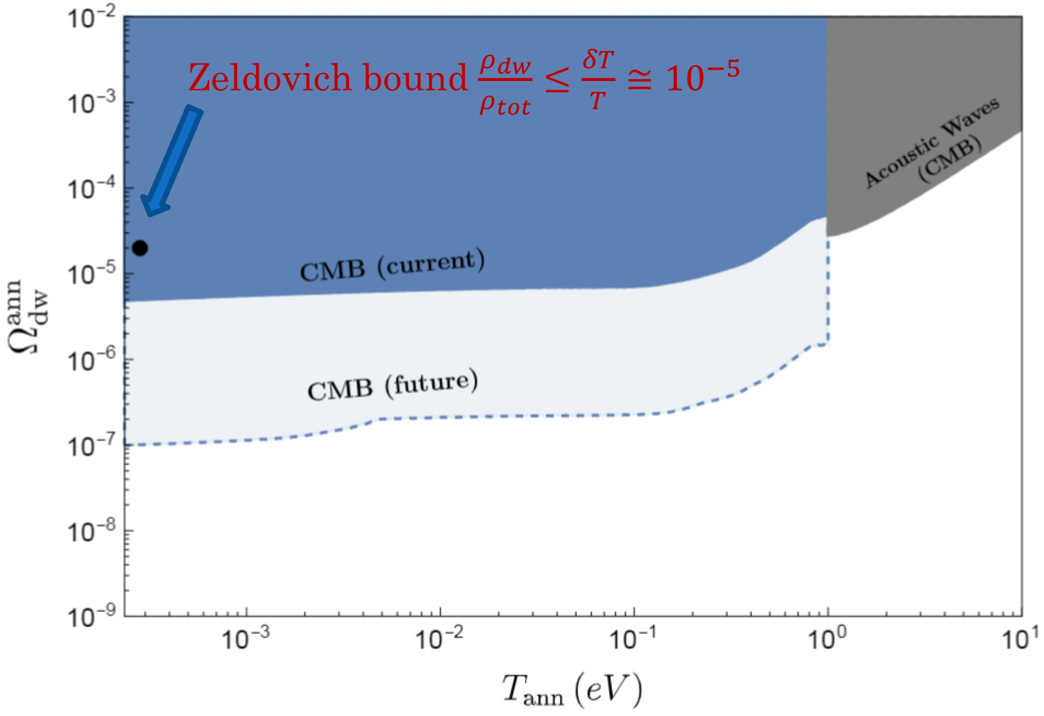

Summary of part II

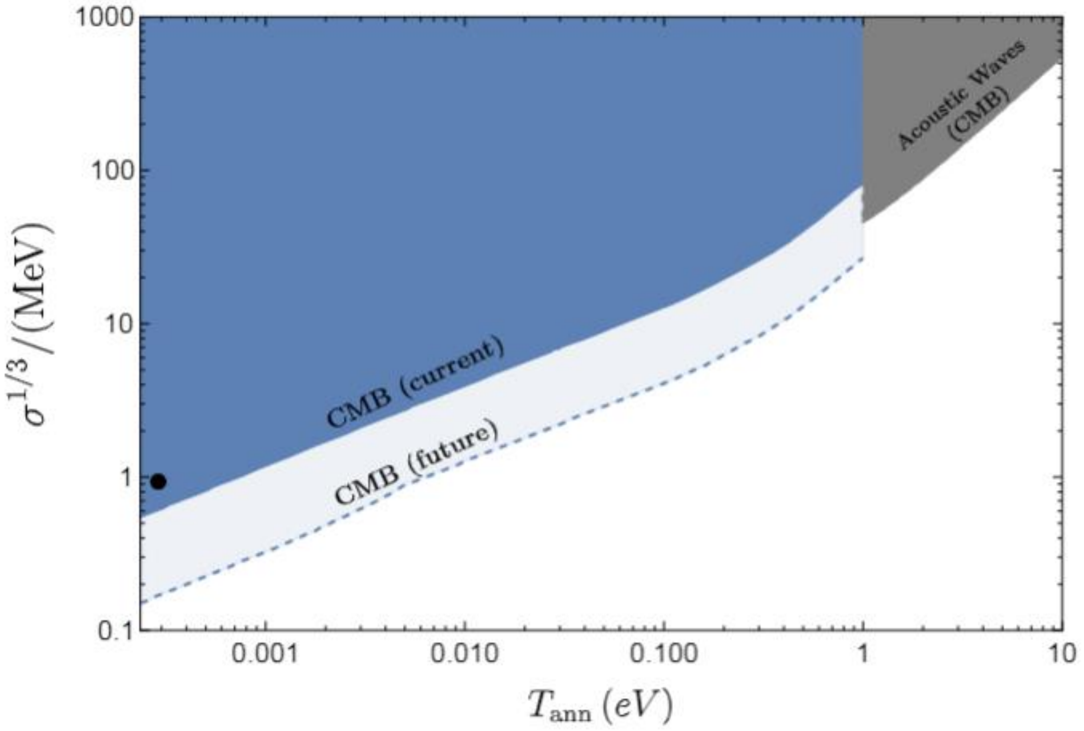

- Isotropic birefringence → mean value, average over all sky
- Anisotropic part → spectrum which peaks at the horizon
- Anisotropies + tomography → allow us to distinguish different annihilation/formation scenarios
- Effect on B-modes → first bounds on DW network that annihilate after recombination

Future works:

- Effect of the network on the TT-spectrum
- Birefringence non-linearities (beyond power spectrum)
- Other types of network
- New observables?

Thank you for your attention!

sgasparotto@ifae.es

Aligned case

The expectation changes if the initial value is not randomly distributed around zero but it has a preferable sign.

In this case $\langle\beta\rangle \approx 0.033\, N \frac{\langle\phi_{in}\rangle}{\langle f_a\rangle}$ deg $\rightarrow N \sim 10 \frac{\langle f_a\rangle}{\langle\phi_{in}\rangle}$

Thus the abundance gives

$$\Omega_\phi \cong \frac{3}{8} N \left(\frac{\langle\phi_{in}\rangle^2}{M_{pl}^2} + \frac{\sigma_\phi^2}{M_{pl}^2}\right) \sim \frac{30}{8} \frac{\langle f_a\rangle}{\langle\phi_{in}\rangle} \left(\frac{\langle\phi_{in}\rangle^2}{M_{pl}^2} + \frac{\sigma_\phi^2}{M_{pl}^2}\right)$$

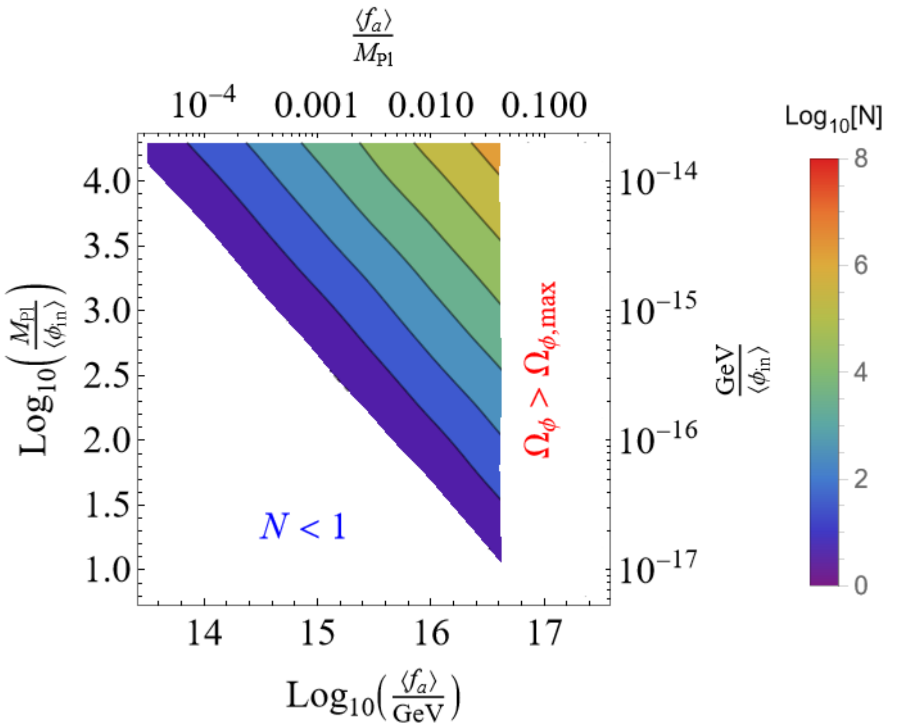

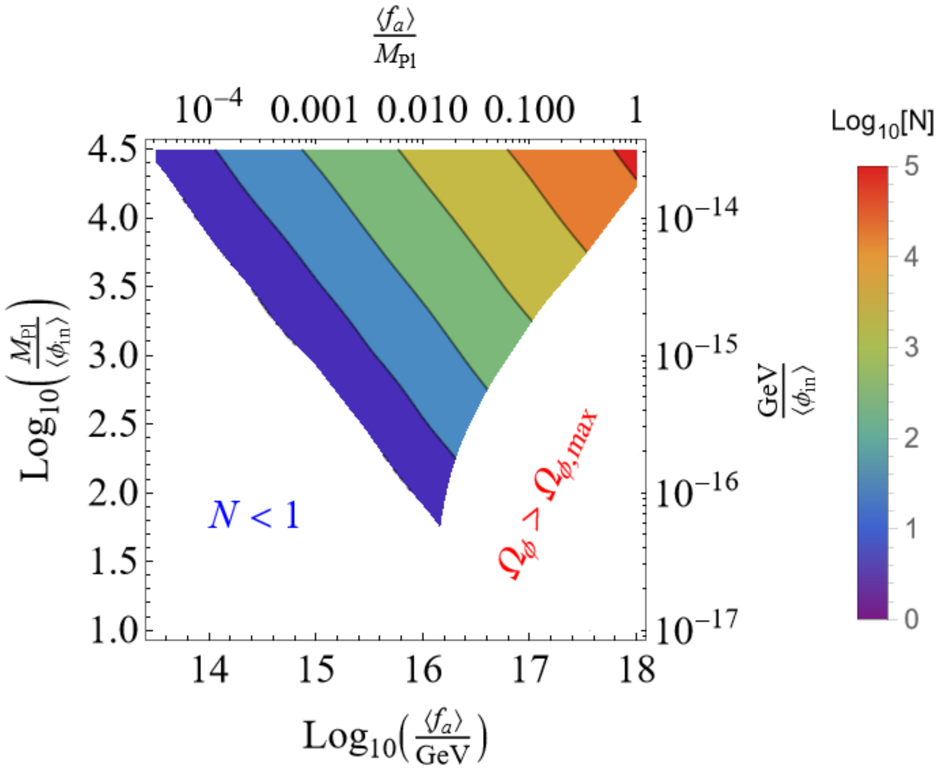

Aligned case

The expectation changes if the initial value is not randomly distributed around zero but it has a preferable sign.

In this case $\langle\beta\rangle \approx 0.033\,\mathrm{N}\frac{\langle\phi_{\mathrm{in}}\rangle}{\langle f_a\rangle}\,\mathrm{deg} \rightarrow \mathrm{N}{\sim}10\frac{\langle f_a\rangle}{\langle\phi_{\mathrm{in}}\rangle}$

Thus the abundance gives

$$\Omega_\phi \cong \frac{3}{8}\mathrm{N}\left(\frac{\langle\phi_{\mathrm{in}}\rangle^2}{M_{\mathrm{pl}}^2}+\frac{\sigma_\phi^2}{M_{\mathrm{pl}}^2}\right) \sim \frac{30}{8}\frac{\langle f_a\rangle}{\langle\phi_{\mathrm{in}}\rangle}\left(\frac{\langle\phi_{\mathrm{in}}\rangle^2}{M_{\mathrm{pl}}^2}+\frac{\sigma_\phi^2}{M_{\mathrm{pl}}^2}\right)$$

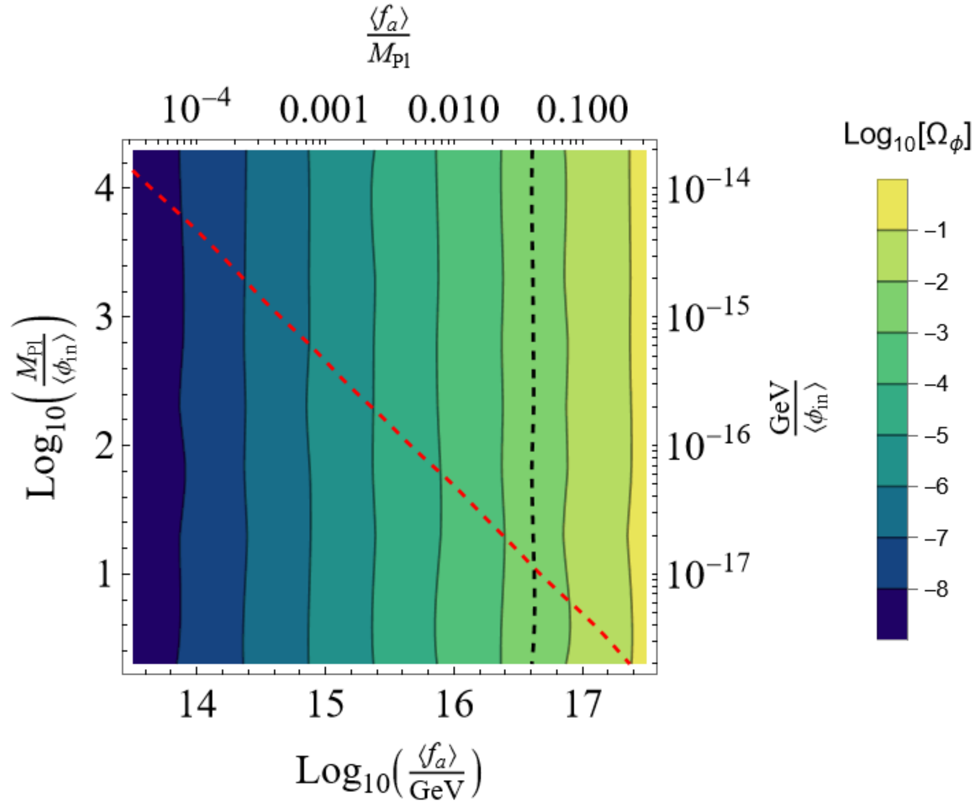

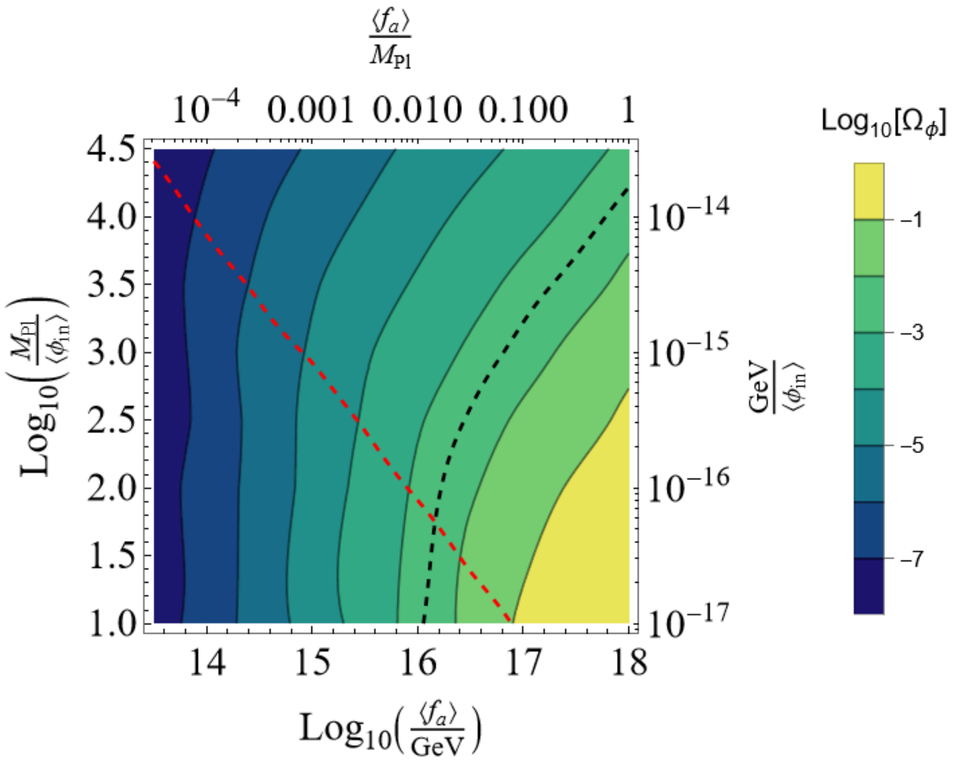

Birefringence Tomography and Evolution of DWs

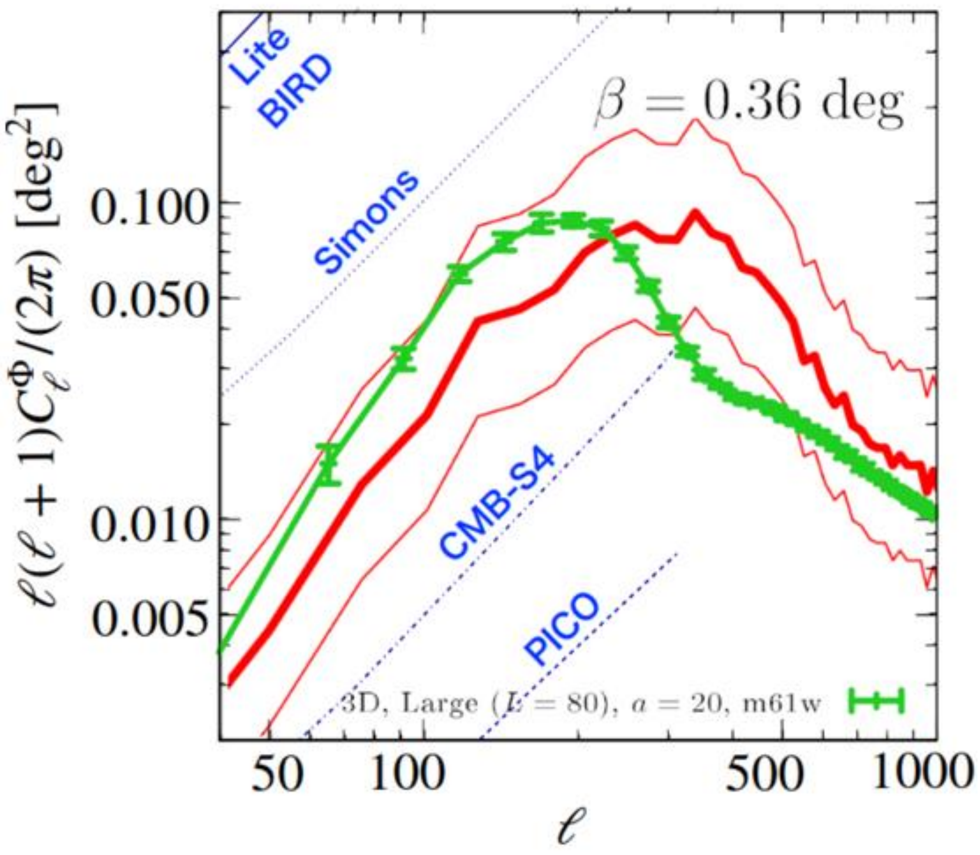

With the tomographic information of the isotropic and anisotropic birefringence, we can distinguish between different evolutions of the network:

Formation \ Annihilation	$z_{\rm rec} > z_{\rm ann} > z_{\rm rei}$	$z_{\rm rei} > z_{\rm ann} > 0$
Isotropic Birefringence:		
$z_{\rm f} > z_{\rm ann}$	$\beta_{\rm rec} \neq \beta_{\rm rei} = 0$	$\beta_{\rm rec} \simeq \beta_{\rm rei} \neq 0$
Anisotropic Birefringence:		
$z_{\rm f} > z_{\rm rec}$	$C^{\beta\beta}_{\rm DW}\|_{\rm rec}$, $C^{\beta\beta}_{\rm DW}\|_{\rm rei} \sim 0$	$C^{\beta\beta}_{\rm DW}\|_{\rm rec}$, $C^{\beta\beta}_{\rm DW}\|_{\rm rei}$
$z_{\rm rec} > z_{\rm f} > z_{\rm rei}$	$C^{\beta\beta}_{\rm IC}\|_{\rm rec}$, $C^{\beta\beta}_{\rm DW}\|_{\rm rei} \sim 0$	$C^{\beta\beta}_{\rm IC}\|_{\rm rec}$, $C^{\beta\beta}_{\rm DW}\|_{\rm rei}$
$z_{\rm rei} > z_{\rm f} > 0$	//	$C^{\beta\beta}_{\rm IC}\|_{\rm rec}$, $C^{\beta\beta}_{\rm IC}\|_{\rm rei}$

The issue with DWs initial conditions at large scales

To generate domain walls the spread of the initial field value $\theta_i = \frac{\phi_i}{f_a}$ must be $O(\pi)$ ⟶ different choices of initial conditions: white noise, thermal spectrum or scale invariant…

The **scale invariant case** (fluctuations have inflationary origin) is qualitatively different → super horizon fluctuations make the **network more stable** Gonzales et all 2023

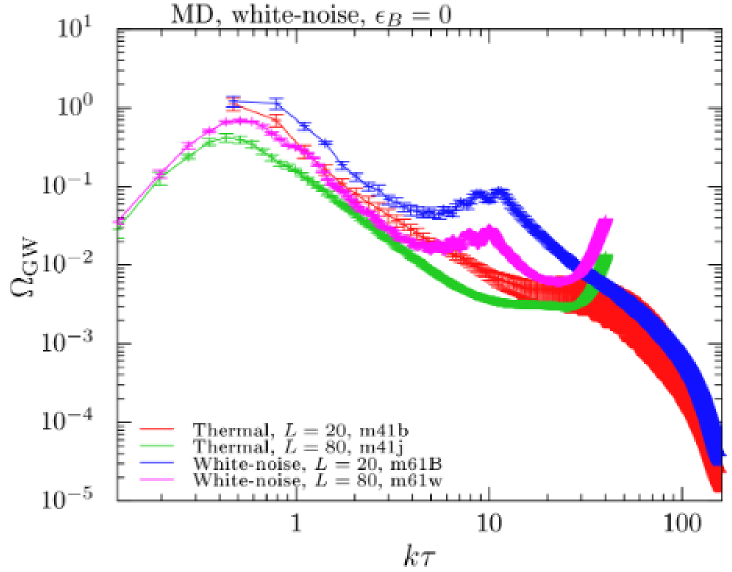

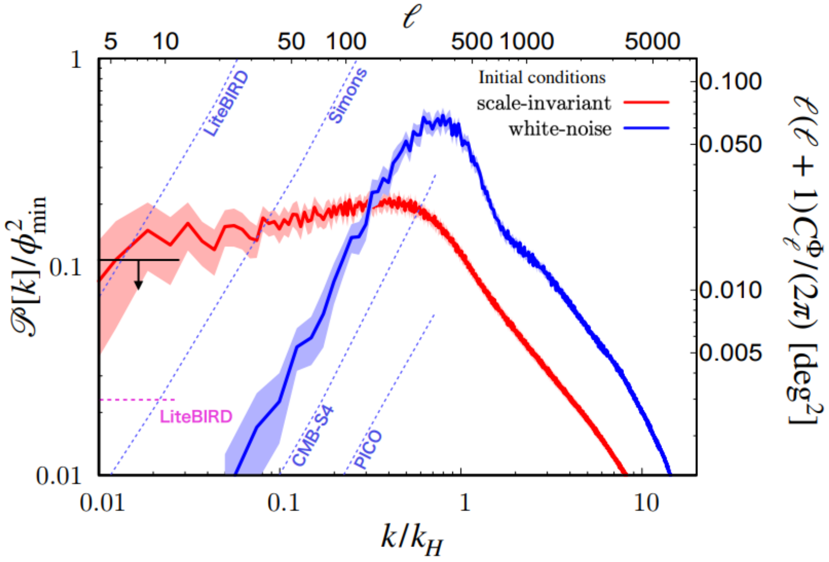

Big impact on the anisotropic, but not in the gravitational wave spectrum!

The main contribution at a large scale mainly comes from motion at smaller scales.

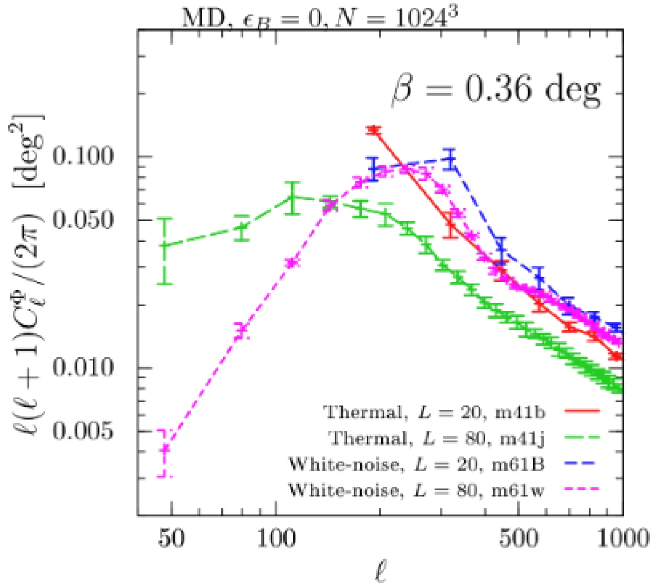

How is that related to observables?

Alessandro Greco et al (2022) 2211.06380

$$
\begin{aligned}
C_{\ell,\mathrm{rot}}^{EE}\big|_{xz} = {} & \left(1-2V_\alpha\big|_{xx}-2V_\alpha\big|_{zz}\right)\left[C_\ell^{EE}\big|_{xz}\cos(2\alpha_{0,x})\cos(2\alpha_{0,z})+C_\ell^{BB}\big|_{xz}\sin(2\alpha_{0,x})\sin(2\alpha_{0,z})\right] \\
& +\frac{2}{2\ell+1}\sum_{L_1L_2} I_{\ell L_1 L_2}^{2,-2,0}\Big(C_{L_2}^{\alpha\alpha}\big|_{xz} I_{\ell L_1 L_2}^{2,-2,0}\Big\{C_{L_1}^{EE}\big|_{xz}\left[\cos(2\alpha_{0,x}-2\alpha_{0,z})-(-1)^{\ell+L_1+L_2}\cos(2\alpha_{0,x}+2\alpha_{0,z})\right] \\
& \qquad +C_{L_1}^{BB}\big|_{xz}\left[\cos(2\alpha_{0,x}-2\alpha_{0,z})+(-1)^{\ell+L_1+L_2}\cos(2\alpha_{0,x}+2\alpha_{0,z})\right]\Big\} \\
& \qquad +C_{L_1}^{\alpha E}\big|_{xz}C_{L_2}^{\alpha E}\big|_{zx} I_{\ell L_1 L_2}^{2,0,-2}\left[\cos(2\alpha_{0,x}-2\alpha_{0,z})-(-1)^{\ell+L_1+L_2}\cos(2\alpha_{0,x}+2\alpha_{0,z})\right]\Big),
\end{aligned}
$$

$$
\begin{aligned}
C_{\ell,\mathrm{rot}}^{BB}\big|_{xz} = {} & \left(1-2V_\alpha\big|_{xx}-2V_\alpha\big|_{zz}\right)\left[C_\ell^{BB}\big|_{xz}\cos(2\alpha_{0,x})\cos(2\alpha_{0,z})+C_\ell^{EE}\big|_{xz}\sin(2\alpha_{0,x})\sin(2\alpha_{0,z})\right] \\
& +\frac{2}{2\ell+1}\sum_{L_1L_2} I_{\ell L_1 L_2}^{2,-2,0}\Big(C_{L_2}^{\alpha\alpha}\big|_{xz} I_{\ell L_1 L_2}^{2,-2,0}\Big\{C_{L_1}^{EE}\big|_{xz}\left[\cos(2\alpha_{0,x}-2\alpha_{0,z})+(-1)^{\ell+L_1+L_2}\cos(2\alpha_{0,x}+2\alpha_{0,z})\right] \\
& \qquad +C_{L_1}^{BB}\big|_{xz}\left[\cos(2\alpha_{0,x}-2\alpha_{0,z})-(-1)^{\ell+L_1+L_2}\cos(2\alpha_{0,x}+2\alpha_{0,z})\right]\Big\} \\
& \qquad +C_{L_1}^{\alpha E}\big|_{xz}C_{L_2}^{\alpha E}\big|_{zx} I_{\ell L_1 L_2}^{2,0,-2}\left[\cos(2\alpha_{0,x}-2\alpha_{0,z})+(-1)^{\ell+L_1+L_2}\cos(2\alpha_{0,x}+2\alpha_{0,z})\right]\Big),
\end{aligned}
$$

$$
\begin{aligned}
C_{\ell,\mathrm{rot}}^{EB}\big|_{xz} = {} & \left(1-2V_\alpha\big|_{xx}-2V_\alpha\big|_{zz}\right)\left[C_\ell^{EE}\big|_{xz}\cos(2\alpha_{0,x})\sin(2\alpha_{0,z})-C_\ell^{BB}\big|_{xz}\sin(2\alpha_{0,x})\cos(2\alpha_{0,z})\right] \\
& +\frac{2}{2\ell+1}\sum_{L_1L_2} I_{\ell L_1 L_2}^{2,-2,0}\Big(C_{L_2}^{\alpha\alpha}\big|_{xz} I_{\ell L_1 L_2}^{2,-2,0}\Big\{C_{L_1}^{BB}\big|_{xz}\left[\sin(2\alpha_{0,x}-2\alpha_{0,z})-(-1)^{\ell+L_1+L_2}\sin(2\alpha_{0,x}+2\alpha_{0,z})\right] \\
& \qquad -C_{L_1}^{EE}\big|_{xz}\left[\sin(2\alpha_{0,x}-2\alpha_{0,z})+(-1)^{\ell+L_1+L_2}\sin(2\alpha_{0,x}+2\alpha_{0,z})\right]\Big\} \\
& \qquad -C_{L_1}^{\alpha E}\big|_{xz}C_{L_2}^{\alpha E}\big|_{zx} I_{\ell L_1 L_2}^{2,0,-2}\left[\sin(2\alpha_{0,x}-2\alpha_{0,z})-(-1)^{\ell+L_1+L_2}\sin(2\alpha_{0,x}+2\alpha_{0,z})\right]\Big),
\end{aligned}
$$

$$
C_{\ell,\mathrm{rot}}^{TE}\big|_{xz} = \left(1-2V_\alpha\big|_{zz}\right)\cos(2\alpha_{0,z})C_\ell^{TE}\big|_{xz},
$$

Monodromic Dark Energy Model

Panda et al. (2011)

$$V = \frac{\mu^4}{f_a}\phi \rightarrow \frac{1}{\rho_c}\frac{dV}{d\phi} = s = \frac{\mu^4/f_a}{3M_{Pl}H_0^2}$$

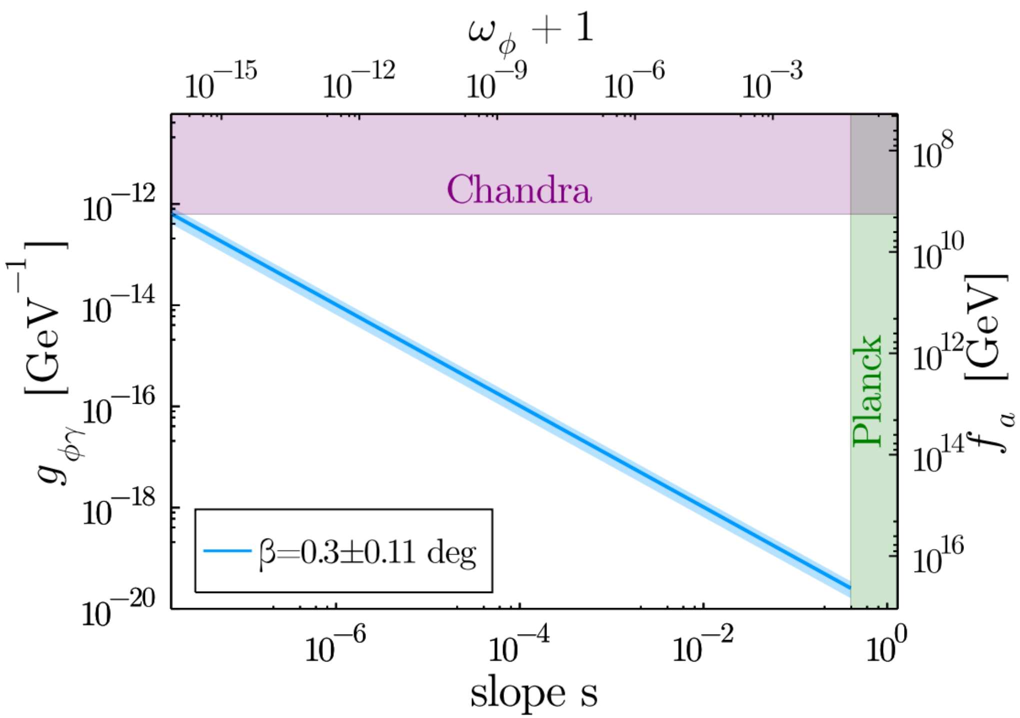

SG & Ippei Obata 2203.09409

Inferred axion-photon coupling from the measured birefringence angle for different slopes:

$$g_{\phi\gamma} = 2.57 \times 10^{-20}\mathrm{GeV}^{-1}\left(\frac{|\beta|}{0.30\mathrm{deg}}\right)\left(\frac{0.4}{s}\right)$$

Or different equation of state:

$$g_{\phi\gamma} = 2.57 \times 10^{-20}\mathrm{GeV}^{-1}\left(\frac{|\beta|}{0.30\mathrm{deg}}\right)\left(\frac{0.05}{\omega_\phi + 1}\right)^{1/2}$$

Tightest constraint on the axion-photon coupling from Chandra X-ray observatories: Reynés et al. (2021)

$$g_{\phi\gamma} \leq 6.3 \times 10^{-13}\mathrm{GeV}^{-1} \xrightarrow{yields} \omega_\phi + 1 \geq 2.67 \times 10^{-16}\left(\frac{|\beta|}{0.30\mathrm{deg}}\right)^2$$

$$\frac{f_a}{c_{\gamma\phi}} = 4.52 \times 10^{16}\mathrm{GeV}\left(\frac{0.30\mathrm{deg}}{|\beta|}\right)\left(\frac{\omega_\phi+1}{0.05}\right)^{1/2}$$